Available online at www.sciencedirect.com

SciVerse ScienceDirect

Mathematics and Computers in Simulation xxx (2011) xxx–xxx

MATHEMATICS AND COMPUTERS IN SIMULATION

www.elsevier.com/locate/matcom

Original article

Numerical solution of the ‘classical’ Boussinesq system

D.C. Antonopoulos [a], V.A. Dougalis [a,b,*]

[a] Department of Mathematics, University of Athens, 15784 Zographou, Greece
[b] Institute of Applied and Computational Mathematics, FORTH, 71110 Heraklion, Greece

Received 24 November 2009; received in revised form 13 September 2011; accepted 16 September 2011

Abstract

We consider the ‘classical’ Boussinesq system of water wave theory, which belongs to the class of Boussinesq systems modelling two-way propagation of long waves of small amplitude on the surface of water in a horizontal channel. (We also consider its completely symmetric analog.) We discretize the initial-boundary-value problem for these systems, corresponding to homogeneous Dirichlet boundary conditions on the velocity variable at the endpoints of a finite interval, using fully discrete Galerkin-finite element methods of high accuracy. We use the numerical schemes as exploratory tools to study the propagation and interactions of solitary-wave solutions of these systems, as well as other properties of their solutions.

Keywords: Water waves; ‘Classical’ Boussinesq systems; Initial-boundary-value problems; Fully discrete Galerkin-finite element methods; Solitary waves

1. Introduction

We consider the so-called ‘classical’ Boussinesq system (CB)

$$\begin{aligned} &\eta_t + u_x + (\eta u)_x = 0, \\ &u_t + \eta_x + u u_x - \frac{1}{3} u_{xxt} = 0, \end{aligned} \tag{1.1}$$

for $x \in \mathbb{R}$, $t > 0$, supplemented by the initial conditions

$$\eta(x, 0) = \eta_0(x), \qquad u(x, 0) = u_0(x), \tag{1.2}$$

where η_0, u_0 are given real functions on $\mathbb{R}$. The system (1.1) is a Boussinesq-type approximation of the two-dimensional Euler equations that models two-way propagation of long waves of small amplitude on the surface of an incompressible, inviscid fluid in a uniform horizontal channel of finite depth. The variables in (1.1) and (1.2) are nondimensional and unscaled: x and t are proportional to position along the channel and time, respectively, and $\eta(x, t)$ and $u(x, t)$ are proportional to the elevation of the free surface above the level of rest $y = 0$, and to the horizontal velocity of the fluid at a height $y = -1 + (1 + \eta(x, t))/\sqrt{3}$, respectively. (In terms of these variables the bottom of the channel is at $y = -1$.)

* Corresponding author at: Department of Mathematics, University of Athens, 15784 Zographou, Greece. Tel.: +30 210 7276311; fax: +30 210 7276398.
E-mail address: doug@math.uoa.gr (V.A. Dougalis).

0378-4754/$36.00 © 2011 IMACS. Published by Elsevier B.V. All rights reserved.
doi:10.1016/j.matcom.2011.09.006

The CB system is a member of a general family of Boussinesq systems derived in [11], that are approximations to the Euler equations of the same order and written in nondimensional, unscaled variables as

$$\begin{aligned} &\eta_t + u_x + (\eta u)_x + a u_{xxx} - b\eta_{xxt} &= 0, \\ &u_t + \eta_x + u u_x + c\eta_{xxx} - d u_{xxt} &= 0, \end{aligned} \tag{1.3}$$

where $a = (\theta^2 - 1/3)\nu/2$, $b = (\theta^2 - 1/3)(1 - \nu)/2$, $c = (1 - \theta^2)\mu/2$, $d = (1 - \theta^2)(1 - \mu)/2$, where ν and μ are modelling parameters and $0 \le \theta \le 1$. In the case of the CB we have $\mu = 0$ and $\theta^2 = 1/3$.

The CB system was formally derived from the Euler equations, in the appropriate parameter regime, in [27,29,33]. Specifically, if $\varepsilon = A/h_0$ and $\sigma = h_0/\lambda$, where A is a typical wave amplitude, h_0 is the depth of the channel and λ a typical wavelength, and it is assumed that $\varepsilon \ll 1$, $\sigma \ll 1$, with $\varepsilon = \sigma^2$ for definiteness (so that the Stoke's number $S = \varepsilon/\sigma^2 = 1$), appropriate nondimensionalization and scaling of the Euler equations followed by expansions in powers of ε yield formally that

$$\begin{aligned} &\eta_t + u_x + \varepsilon(\eta u)_x = O(\varepsilon^2), \\ &u_t + \eta_x + \varepsilon u u_x - \frac{1}{3}\varepsilon u_{xxt} = O(\varepsilon^2), \end{aligned}$$

in nondimensional, scaled variables, denoted again by η, u, x, t. Replacing the right-hand side of the above equations by zero we obtain the *scaled CB system*

$$\begin{aligned} &\eta_t + u_x + \varepsilon(\eta u)_x = 0, \\ &u_t + \eta_x + \varepsilon u u_x - \frac{1}{3}\varepsilon u_{xxt} = 0, \end{aligned} \tag{1.4}$$

for $x \in \mathbb{R}$, $t > 0$. As pointed out in [33,24], in his work in the 1870s Boussinesq derived a system very close to (1.4) but with the term $-\varepsilon u_{xxt}/3$ replaced (in our notation) by $\varepsilon\eta_{xtt}/3$. In view of the lower-order relation $\eta_t = -u_x + O(\varepsilon)$ implied by (1.4), one may then derive the system in its present form, which is mathematically more tractable.

Existence and uniqueness of solution of the initial-value problem (ivp) (1.1) and (1.2) was studied by Schonbek [30] and Amick [3]. In these papers global existence and uniqueness was established for infinitely differentiable initial data of compact support. In [12] the theory of [30,3] was used to establish that given initial data $(\eta_0, u_0) \in H^s \times H^{s+1}$, where $s \ge 1$, and such that $\inf_{x\in\mathbb{R}}\eta_0(x) > -1$, there is a unique solution (η, u), which, for any $T > 0$, lies in $C(0, T; H^s) \times C(0, T; H^{s+1})$. (Here $H^s = H^s(\mathbb{R})$ is the usual, L^2-based Sobolev space of functions on $\mathbb{R}$ and $C(0, T; X)$ denotes the space of functions $\phi = \phi(t)$ that for each $t \in [0, T]$ have values in the Banach space X and are such that the map $[0, T] \to \| \phi \|_X$ is continuous.) As a consequence of this global existence-uniqueness result and of the theory in [13,2], one may rigorously formulate a precise sense in which the scaled system (1.4) is an $O(\varepsilon^2)$ approximation to the Euler equations. Specifically, one may prove that solutions of (1.4) with suitable initial data approximate, in appropriate norms, analogous solutions of the Euler equations, in the same scaling, with an error of $O(\varepsilon^2 t)$ uniformly for $t \in [0, T_\varepsilon]$, where T_ε is of $O(1/\varepsilon)$.

It is well known that the CB system possesses classical solitary-wave solutions. These are travelling wave solutions of (1.1) of the form $\eta(x, t) = \eta_s(x + x_0 - c_s t)$, $u(x, t) = u_s(x + x_0 - c_s t)$, where $x_0 \in \mathbb{R}$ and c_s is constant. The functions $\eta_s = \eta_s(\xi)$, $u_s = u_s(\xi)$, $\xi \in \mathbb{R}$, will be assumed to be smooth, positive, even, and decaying monotonically to zero, along with their derivatives, as $\xi \to \pm\infty$. Substituting into (1.1), integrating once and setting the integration constants equal to zero, one obtains the ode's

$$\begin{aligned} &-c_s\eta + u + \eta u = 0, \\ &-c_s u + \eta + \frac{1}{2}u^2 - \frac{c_s}{3}u'' = 0, \end{aligned}$$

where we have denoted η_s, u_s simply by η, u and $' = d/d\xi$. (We may assume that $c_s > 0$ since if (η, u) is a solution of this system of ode's for some $c_s > 0$, then $(\eta, -u)$ is also a solution propagating with speed $-c_s$.) As opposed to the case of a more general *a b c d* system (1.3), wherein the resulting system of second-order nonlinear ode's is coupled, the above ode system decouples and may be written in the form

$$\eta = \frac{u}{c_s - u}, \tag{1.5a}$$

Please cite this article in press as: D.C. Antonopoulos, V.A. Dougalis. Numerical solution of the 'classical' Boussinesq system, Math. Comput. Simul. (2011), doi:10.1016/j.matcom.2011.09.006

$$-c_s u + \frac{u}{c_s - u} + \frac{1}{2}u^2 - \frac{c_s}{3}u'' = 0. \tag{1.5b}$$

The second equation may be studied by a straightforward phase plane analysis, cf. [24,18], and yields existence and uniqueness of solitary waves for any value of $c_s > 1$.

Solitary waves play an important role in the evolution and long-time asymptotic behavior of solutions of the ivp (1.1) and (1.2) that emanate from initial data that decays sufficiently fast at infinity. Such solutions are resolved as t increases into series of solitary waves followed by oscillatory dispersive tails of small amplitude. This *resolution* property has been rigorously proved by inverse scattering theory for integrable, one-way models such as the KdV equation, and has been observed numerically in many other examples of nonlinear dispersive wave propagation, and in particular in the case of Boussinesq systems, cf. e.g. [10,4,5,26,20,8]. It may be viewed as a manifestation of the *stability* of solitary waves. It is well known, cf. e.g. [24,20], that the classical variational theory for studying orbital stability of solitary waves does not work in the case of the Boussinesq systems, and that there does not exist yet a rigorous proof of their asymptotic stability. However, linearized 'convective' asymptotic stability of the solitary waves of the CB was established in [24]. A detailed numerical study of various stability properties of the solitary waves of the Bona-Smith family of Boussinesq systems has been carried out in [20]. (Similar numerical experiments have been performed by the authors of the present paper in the case of the solitary waves of the CB system, which appear again to be asymptotically stable under a variety of perturbations.)

In this paper we shall solve numerically the following initial-boundary-value problem (ibvp) for CB: For some $L > 0$ we seek $\eta = \eta(x, t)$, $u = u(x, t)$ defined for $0 \le x \le L$, $t \ge 0$, that satisfy (1.1) for $0 \le x \le L$, $t \ge 0$, the initial conditions (1.2) for $0 \le x \le L$, and the boundary conditions

$$u(0, t) = u(L, t) = 0, \quad t \ge 0. \tag{1.6}$$

This ibvp has been recently analyzed by Adamy [1], who showed that it has weak (distributional) solutions (η, u) in $L^\infty\left(\mathbb{R}^+, L^1(0, L) \times H_0^1(0, L)\right)$ provided that $\eta_0 \in L^1(0, L)$, $u_0 \in H_0^1(0, L)$ with $\inf_{x\in[0,L]}\eta_0(x) > -1$. (Here $H_0^1(0, L)$ denotes the subspace of $H^1(0, L)$ consisting of those elements of $H^1(0, L)$ that vanish at $x = 0$ and $x = L$.) The proof follows the parabolic regularization technique of Schonbek [30]. It should be noted that (1.6) is one kind of boundary conditions that lead to well posed ibvp's in the case of the linearized CB system [22]. The CB system needs only two boundary conditions (b.c.'s) for well-posedness as opposed to the four b.c.'s (for example, Dirichlet b.c.'s on η and u at each end,) required in the case of other Boussinesq systems such as the BBM-BBM [10], and the Bona-Smith systems [9]. Considering the homogeneous Dirichlet boundary conditions (1.6) may be viewed as a first step towards studying their nonhomogeneous analog, where $u(0, t)$ and $u(L, t)$ are given functions of $t \ge 0$, and which would correspond to known measurement of the velocity variable at the two ends of a channel of finite length. This data may be used then as boundary conditions for a numerical scheme, whose results in $[0, L]$ may be compared with experimental values of η and u in order to assess the accuracy of the CB model. This cannot be done if the numerical solution is computed with periodic b.c.'s. (The latter are adequate for the numerical simulation of interactions of solitary waves in the interior of the domain but may not be used e.g. to study the interactions of solitary waves with the boundary.)

In [13], Bona et al. introduced another type of Boussinesq systems that they called *completely symmetric*, obtained from the usual systems of the type (1.3) by a nonlinear change of variables, and having the mathematical advantage that their Cauchy problem is always locally nonlinearly well posed (provided the linearized system is well posed). In addition, solutions of their scaled analogs are $O(\varepsilon^2 t)$ approximations to appropriate solutions of the Euler equations for $t \in [0, T_\varepsilon]$, with $T_\varepsilon = O(1/\varepsilon)$. The completely symmetric analog of CB is the system

$$\begin{aligned} &\eta_t + u_x + \frac{1}{2}(\eta u)_x = 0, \\ &u_t + \eta_x + \frac{3}{2}uu_x + \frac{1}{2}\eta\eta_x - \frac{1}{3}u_{xxt} = 0, \end{aligned} \tag{1.7}$$

which we will call SB in the sequel. Its scaled analog is

$$\begin{aligned} &\eta_t + u_x + \frac{1}{2}\varepsilon(\eta u)_x = 0, \\ &u_t + \eta_x + \frac{3}{2}\varepsilon uu_x + \frac{1}{2}\varepsilon\eta\eta_x - \frac{1}{3}\varepsilon u_{xxt} = 0. \end{aligned} \tag{1.8}$$

If we consider (1.7) on the finite spatial interval [0, L] with the homogeneous boundary conditions (1.6), it turns out that the solution of the resulting ibvp satisfies the conservation property

$$\|\eta(t)\|^2 + \|u(t)\|^2 + \frac{1}{3}\|u_x(t)\|^2 = \|\eta_0\|^2 + \|u_0\|^2 + \frac{1}{3}\|u_0'\|^2, \tag{1.9}$$

for $t \geq 0$, which simplifies the study of its well-posedness and the estimation of the errors of its numerical approximations, cf. [7]. The SB system has solitary waves, that are solutions of the ode's

$$\eta = \frac{2u}{2c_s - u}, \tag{1.10a}$$

$$-c_s u + \eta + \frac{3}{4}u^2 + \frac{1}{4}\eta^2 - \frac{c_s}{3}u'' = 0. \tag{1.10b}$$

In the paper at hand we shall study, by numerical means, various properties of the solutions of the CB and the SB systems, paying particular attention to simulations of the generation, propagation, and interactions of their solitary waves. Numerical simulations of solitary wave interactions of the CB system were also performed with spectral methods in [25,26], and with finite element methods in [4,5]. (For numerical work on other Boussinesq systems of the type (1.3) we refer the reader to e.g. [25,10,6,4,26,23,15,16,20].) It should be noted that the CB system has been extensively used in the engineering fluid mechanics literature for dispersive, nonlinear wave modelling and computations, starting with the pioneering papers of Peregrine [27,28].

In Section 2 of the paper at hand we describe the numerical scheme that will be used in our simulations. We consider the ibvp's for CB and SB with the homogeneous boundary conditions (1.6) and we discretize them in space using the standard Galerkin-finite element method with continuous, piecewise linear functions and cubic splines. (In the computations of Section 3 we use cubic splines.) The resulting semidiscrete systems of ode's are discretized in the temporal variable using the classical, explicit, four-stage Runge–Kutta scheme of order four. It turns out that these ode systems are mildly stiff, so that a condition of the form $k = O(h)$ is needed for stability, where k is the time step and h the spatial meshlength. This stability condition is not severe and it allows using an explicit time-stepping procedure, thus avoiding the more costly implicit methods that require solving nonlinear systems of equations at each time step.

The error analysis of these numerical schemes is of considerable interest due to the loss of optimal order of accuracy in the discretization of the 'hyperbolic' first p.d.e. of the systems (1.1) or (1.7) on a finite interval in the presence of non-periodic boundary conditions. (The loss of optimal order of accuracy in standard Galerkin approximations of first-order hyperbolic problems is well known, cf. e.g. [21].) In our case, the facts that the other pde of both systems has the dispersive term $-u_{xxt}$, and that u vanishes at the endpoints of [0, L] help us to prove, in the case of uniform spatial meshlength h, improved error estimates e.g. of the form $\max_{0\leq t\leq T}\|\eta(t) - \eta_h(t)\| \leq Ch^{3.5}\sqrt{\ln 1/h}$, $\max_{0\leq t\leq T}\|u(t) - u_h(t)\| \leq Ch^4\sqrt{\ln 1/h}$, where η_h, u_h are the standard Galerkin cubic spline semidiscrete approximations to η, u, respectively, $\|\cdot\|$ denotes the L^2 norm on [0, L], and C is a constant independent of h. In Section 2 we state this and other error estimates for our numerical schemes; their proofs will appear elsewhere, but the interested reader may consult [7].

In Section 3 we present the results of numerical experiments that we performed using the cubic spline – Runge–Kutta fully discrete scheme as an exploratory tool for investigating various properties of solutions of CB and SB. In several numerical experiments involving solitary waves and their interactions, we compute on fairly large spatial intervals [0, L] so that there are no unwanted interactions with the boundaries. In Section 3.1 we study the resolution into solitary waves propagating in both directions emanating from an initial Gaussian 'heap' of water, and make some remarks on the number of solitary waves that are produced. We recall the process of iterative 'cleaning' used to generate solitary waves numerically [10,20], and find analytic relations between the speed c_s and the amplitude A_s of solitary waves for CB and SB.

In Section 3.2 we study numerically head-on collisions between solitary waves of equal and unequal height for both systems. The results are qualitatively the same as those observed in similar numerical experiments in the case of other Boussinesq systems and the Euler equations [10,8,19]. For both CB and SB there seems to occur a slight, permanent loss of height of the solitary wave of larger amplitude after the interaction. In Section 3.3 we turn to overtaking collisions of solitary waves travelling in the same direction. Such collisions have been studied in detail for one-way models numerically, and by the inverse scattering transform in the integrable case. The results in the case of CB and SB qualitatively agree with those of similar interactions of solitary waves of other Boussinesq systems, including the appearance of a large-wavelength, small-amplitude, dispersive wavelet that travels in a direction opposite to that of the motion of the solitary waves.

In Section 3.4 we study numerically what happens when a solitary wave of the CB or the SB system collides with the boundary point, say at $x = L$, where $u = 0$ holds. Although the condition $\eta_x = 0$ is not imposed as a boundary condition on the pde system or the numerical scheme, it appears that the numerical approximation of $\eta_x(L, t)$ tends to zero as $h \to 0$. Hence, in the case of this type of Boussinesq systems as well, it appears that reflection of a solitary wave from a vertical wall (where only $u = 0$ is imposed now) is equivalent to (one half) of the head-on collision of the solitary wave with its symmetric image of opposite velocity, at the center of which $\eta_x = 0$ and $u = 0$ hold due to symmetry.

In Section 3.5 we present the results of numerical experiments indicating that solutions of the ibvp's for the CB and SB systems with the boundary conditions (1.6) may blow up in finite time provided the initial conditions are suitable large, but still satisfy $1 + \eta_0 > 0$ on $[0, L]$. Thus, it appears that although the Cauchy problem for these systems is well posed in classes of functions that decay fast enough at infinity, solutions of the ibvp on a finite interval may develop singularities in finite time, something which is not precluded by the existing well-posedness theory [1]. Finally, in Section 3.6 we compare solutions of the ibvp's for the *scaled* CB and SB systems for appropriate initial data and small values of the parameter ε, as t grows, in order to test the consistency of the theory of [13,2] (which is properly valid for the Cauchy problem) in the case of a finite interval under the b.c.'s (1.6).

Preliminary results of some numerical experiments included in this paper originally appeared in [4,5].

2. Numerical schemes

For the convenience of the reader we rewrite here the ibvp's that will be solved numerically. In the case of the CB system, we seek $\eta = \eta(x, t)$, $u = u(x, t)$ for $0 \le x \le L$, $t \ge 0$, such that

$$\begin{aligned} &\left.\begin{aligned} &\eta_t + u_x + (\eta u)_x = 0, \\ &u_t + \eta_x + u u_x - \frac{1}{3} u_{xxt} = 0, \end{aligned}\right\} \quad 0 \le x \le L, \quad t \ge 0, \\ &\eta(x, 0) = \eta_0(x), \quad u(x, 0) = u_0(x), \quad 0 \le x \le L, \\ &u(0, t) = u(L, t) = 0, \quad t \ge 0, \end{aligned} \tag{2.1}$$

where η_0, u_0 are given real functions on $[0, L]$ with $u_0(0) = u_0(L) = 0$. The analogous ibvp for the SB system is

$$\begin{aligned} &\left.\begin{aligned} &\eta_t + u_x + \frac{1}{2}(\eta u)_x = 0, \\ &u_t + \eta_x + \frac{3}{2} u u_x + \frac{1}{2}\eta\eta_x - \frac{1}{3} u_{xxt} = 0, \end{aligned}\right\} \quad 0 \le x \le L, \ t \ge 0, \\ &\eta(x, 0) = \eta_0(x), \qquad u(x, 0) = u_0(x), \quad 0 \le x \le L, \\ &u(0, t) = u(L, t) = 0, \quad t \ge 0. \end{aligned} \tag{2.2}$$

We shall assume that these systems possess unique solutions in some temporal interval $[0, T]$, which are smooth enough for the purposes of the proofs of the error estimates that will be stated in the sequel.

Let $h > 0$ and $x_i = ih$, $i = 0, 1, \ldots, N$, where N is a positive integer such that $Nh = L$. We consider the finite-dimensional space of continuous piecewise linear functions relative to the partition $\{x_i\}$ of $[0, L]$, i.e. the space

$$S_h^2 = \{\phi \in C[0, L] : \phi|_{[x_i, x_{i+1}]} \in \mathbb{P}_1, \quad 0 \le i \le N-1\},$$

and let $S_{h,0}^2 := S_h^2 \cap H_0^1(0, L)$. In addition, we let S_h^4 denote the space of smooth cubic splines associated with $\{x_i\}$, i.e. put

$$S_h^4 = \{\phi \in C^2[0, L] : \phi|_{[x_i, x_{i+1}]} \in \mathbb{P}_3, \quad 0 \le i \le N-1\},$$

and $S_{h,0}^4 := S_h^4 \cap H_0^1(0, L)$. (Here $\mathbb{P}_k$ are the polynomials of degree at most k.) We will use the notation $S_h = S_h^m$, $S_{h,0} = S_{h,0}^m$ for $m = 2$ or 4 as the case may be. We let $(\cdot, \cdot)$ denote the L^2 inner product on $[0, L]$ and $\|\cdot\|$ the associated norm. For $\phi, \chi \in H^1(0, L)$ we let $a(\phi, \chi) = (\phi, \chi) + (\phi', \chi')/3$.

Please cite this article in press as: D.C. Antonopoulos, V.A. Dougalis. Numerical solution of the 'classical' Boussinesq system, Math. Comput. Simul. (2011), doi:10.1016/j.matcom.2011.09.006

The standard Galerkin semidiscretization of the CB system is defined as follows. We seek $\eta_h : [0, T] \to S_h$, $u_h : [0, T] \to S_{h,0}$ satisfying for $0 \le t \le T$

$$\begin{aligned} &(\eta_{ht}, \phi) + (u_{hx}, \phi) + \big((\eta_h u_h)_x, \phi\big) = 0 \quad \forall \phi \in S_h, \\ &a(u_{ht}, \chi) + (\eta_{hx}, \chi) + (u_h u_{hx}, \chi) = 0 \quad \forall \chi \in S_{h,0}, \end{aligned} \tag{2.3}$$

where $\eta_h(0) \in S_h$, $u_h(0) \in S_{h,0}$ are approximations of η_0, u_0, respectively. We usually take, in the case $m = 2$ of piecewise linear functions $\eta_h(0) = I_h\eta_0$, $u_h(0) = I_{h,0}u_0$, where I_h, $I_{h,0}$ are the interpolant operators onto S_h, $S_{h,0}$, respectively, and in the case $m = 4$ of cubic splines $\eta_h(0) = J_h\eta_0$, $u_h(0) = R_h u_0$, where J_h is the interpolant onto S_h^4 and R_h is the elliptic projection operator onto $S_{h,0}^4$, defined for $v \in H_0^1[0, L]$ by $a(R_h v, \phi) = a(v, \phi)\ \forall \phi \in S_{h,0}^4$.

The analogous semidiscretization of the SB system is defined for $0 \le t \le T$ as

$$\begin{aligned} &(\eta_{ht}, \phi) + (u_{hx}, \phi) + \frac{1}{2}\big((\eta_h u_h)_x, \phi\big) = 0 \quad \forall \phi \in S_h, \\ &a(u_{ht}, \chi) + (\eta_{hx}, \chi) + \frac{3}{2}(u_h u_{hx}, \chi) + \frac{1}{2}(\eta_h \eta_{hx}, \chi) = 0 \quad \forall \chi \in S_{h,0}, \end{aligned} \tag{2.4}$$

with the same initial conditions. It is easy to see that the solution of (2.4) satisfies the discrete analog of (1.9). It is shown in [7] that the ode systems represented by (2.3) and (2.4) have unique solutions for $t \in [0, T]$ and that they satisfy the following L^2-error estimates.

In the case $m = 2$ of piecewise linear functions:

$$\max_{0 \le t \le T} \|\eta(t) - \eta_h(t)\| \le Ch^{3/2}, \qquad \max_{0 \le t \le T} \|u(t) - u_h(t)\| \le Ch^2. \tag{2.5}$$

In the case $m = 4$ of cubic splines:

$$\max_{0 \le t \le T} \|\eta(t) - \eta_h(t)\| \le Ch^{3.5}\sqrt{\ln \frac{1}{h}}, \qquad \max_{0 \le t \le T} \|u(t) - u_h(t)\| \le Ch^4\sqrt{\ln \frac{1}{h}}. \tag{2.6}$$

Here C is a generic constant depending on u, η and T but not on h. We refer the reader to [7] for other error estimates and their proofs.

Some remarks are in order: The estimate for $\eta - \eta_h$ in (2.5) is not of optimal order; one would expect an $O(h^2)$ error bound. However the $O(h^{3/2})$ bound is sharp as numerical experimentation suggests. In the case at hand of the ibvp's (2.1) and (2.2) for our systems, the facts that u vanishes at $x = 0$ and L, the presence of the nice dispersive term $-u_{xxt}$ in the second-listed p.d.e., and the use of the uniform meshes allow us to take advantage of suitable cancellation properties in some error terms and prove the estimates in (2.5). In the case of cubic splines we obtain some further improvement as well.

We turn now to full discretizations of the semidiscrete problems (2.3) and (2.4). Since only the cubic spline spatial discretization will be used in the numerical experiments of the next section, we shall confine ourselves to the case $m = 4$. To match the spatial high order of accuracy we use a fourth-order accurate ode solver, namely the explicit, four-stage, classical Runge–Kutta method, which for the ode ivp $y' = F(t, y)$, $0 \le t \le T$, $y(0) = y^0$, and uniform time step k, where $Mk = T$ for some positive integer M, approximates $y(t^n)$ at $t^n = nk$ by y^n given by the scheme

$$\begin{aligned} &y^{n,1} = y^n, \quad t^{n,1} = t^n \\ &\text{for } i = 2, 3, 4: \\ &y^{n,i} = y^n + k a_i F(t^{n,i-1}, y^{n,i-1}), \quad t^{n,i} = t^n + \tau_i k \\ &y^{n+1} = y^n + k\sum_{j=1}^{4} b_j F(t^{n,j}, y^{n,j}), \end{aligned}$$

where $a_2 = a_3 = 1/2$, $a_4 = 1$, $\tau_2 = \tau_3 = 1/2$, $b_1 = b_4 = 1/6$, $b_2 = b_3 = 1/3$. The implementation of this method in the case of the semidiscrete systems (2.3) and (2.4) is straightforward and the resulting fully discrete schemes require computing right-hand sides and solving four linear systems with the same time-independent matrix (ϕ_i, ϕ_j) and four with $a(\chi_i, \chi_j)$, where $\{\phi_i\}$, $\{\chi_i\}$ are the usual, minimal support bases of S_h^4, $S_{h,0}^4$, respectively, obtained using the B-splines.

It turns out that the o.d.e. systems represented by (2.3) and (2.4) are only mildly stiff. In [7] we prove that for the fully discrete approximations H_h^n, U_h^n, $0 \le n \le M$, of the solutions η and u of either problem (2.1) or (2.2) we have e.g.

$$\max_{0\le n\le M} \|\eta(t^n) - H_h^n\| \le C\left(k^4 + h^{3.5}\sqrt{\ln\frac{1}{h}}\right),$$

$$\max_{0\le n\le M} \|u(t^n) - U_h^n\|_\infty \le C\left(k^4 + h^{3.5}\sqrt{\ln\frac{1}{h}}\right),$$

provided e.g. that $H_h^0 = \eta_h(0)$, $U_h^0 = u_h(0)$ and k/h is sufficiently small. The latter mesh condition is required for the stability of the explicit fourth-order Runge–Kutta scheme. Lower-order explicit time-stepping methods such as the Euler or the improved Euler scheme require stability conditions of the form $k = O(h^2)$, $k = O(h^{4/3})$, respectively.

3. Numerical experiments

In this section we present a series of numerical experiments illustrating the behavior of solutions of the 'classical' Boussinesq system CB and its symmetric counterpart SB in some examples of interest. Unless otherwise stated, we solve throughout the ibvp's (2.1) and (2.2) numerically, using the standard Galerkin method with cubic splines on a uniform mesh for the spatial discretization and the classical, four-stage, fourth-order RK scheme for the time-stepping. As was mentioned in Section 1, solitary-wave solutions of the systems are of major interest, and we shall begin by considering issues of their construction and generation.

3.1. Construction and generation of solitary waves

As a consequence of the formulas (1.5) that define the solitary waves of CB, one may derive in a straightforward way the following relation between the maximum amplitude A_s of the η-solitary wave and its speed c_s:

$$c_s = \frac{\sqrt{6}(1+A_s)}{\sqrt{3+2A_s}} \cdot \frac{\sqrt{(1+A_s)\log(1+A_s) - A_s}}{A_s}. \tag{3.1}$$

This is a consequence of (1.5a,b): Multiplying (1.5b) by u', using (1.5a), and integrating we find

$$\frac{1}{6}u^3 - \frac{c_s}{2}u^2 - \frac{c_s}{6}(u')^2 - u + c_s \ln\frac{c_s - u}{c_s} = 0.$$

Putting $A_s = \max_{\xi\in\mathbb{R}} \eta(\xi) = \eta(0)$, $B_s = \max_{\xi\in\mathbb{R}} u(\xi) = u(0)$, we conclude from (1.5a) and the above that

$$\begin{aligned} &B_s^3 - 3c_sB_s^2 - 6B_s - 6c_s \ln\frac{c_s - B_s}{c_s} = 0,\\ &A_s = \frac{B_s}{c_s - B_s}, \end{aligned} \tag{3.2}$$

from which (3.1) follows. In the case of SB we find from (1.10a,b), in a similar manner, that

$$c_s = 1 + \frac{A_s}{2}, \quad B_s = A_s. \tag{3.3}$$

Hence, in the case of SB we retrieve the speed-amplitude relationship of the one-way models KdV or BBM. In Fig. 1 we compare the graphs of c_s as a function of A_s for CB and SB with the formula $c_s = \sqrt{1 + A_s}$ predicted by Scott Russell [31], on the basis of his experimental observations. Apart from their theoretical importance, the formulas relating c_s, A_s and B_s are useful for checking the accuracy of numerical approximations of solitary waves.

As was mentioned in Section 1, arbitrary initial data that decays suitably at infinity, apparently resolves itself in sequences of solitary waves plus small oscillations. To illustrate this, CB was integrated with initial conditions $\eta_0(x) = \exp(-0.05x^2)$, $u_0(x) = 0$ on $[-300, 300]$ with $h = 0.2$, $k = 0.02$. As Fig. 2 shows, the initial profile divides into two symmetric wavetrains that travel in opposite directions. By $t = 200$ each of these wavetrains has formed three solitary waves followed by small-size, oscillatory dispersive tails. The number of the solitary waves N in each wavetrain increases with the size of the initial data, as Table 1 shows, in which N is recorded at $t = 200$ for various pairs (A, β)

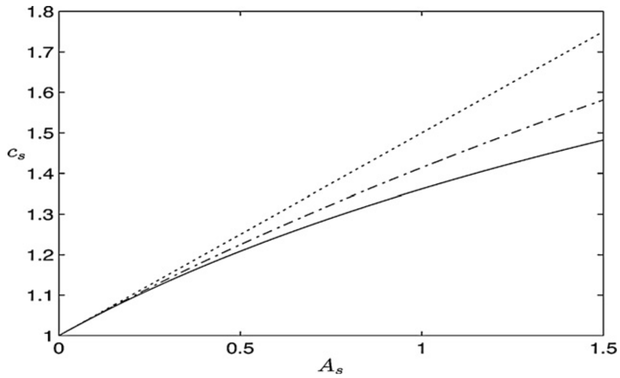

Fig. 1. Speed c_s of η-solitary waves as a function of their amplitude A_s, — CB, ····· SB, —·—·— Scott Russell's prediction.

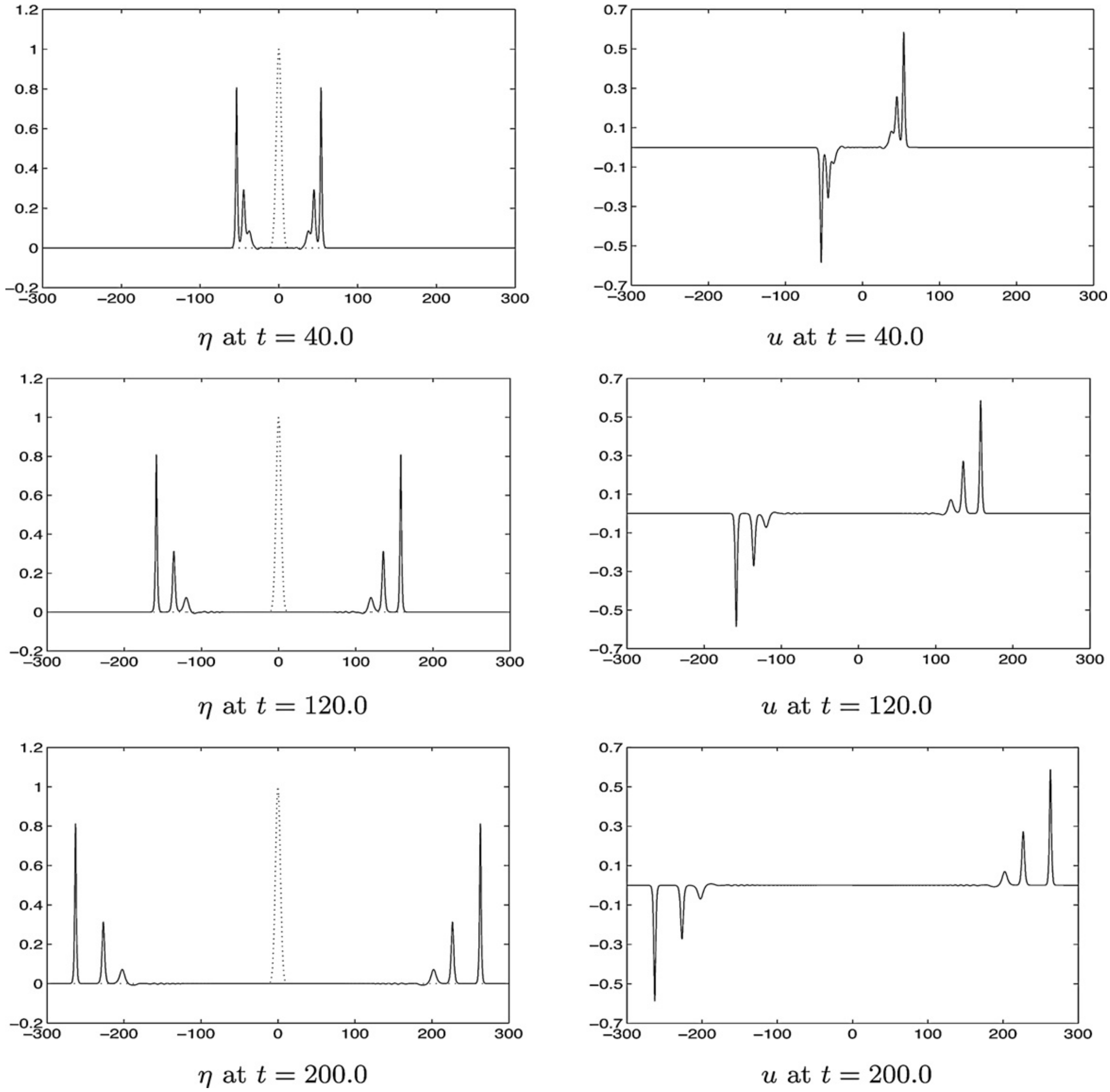

Fig. 2. Resolution of initial data into solitary waves and two-way propagation. CB with $\eta_0(x) = \exp(-0.05x^2)$, $u_0(x) = 0$.

Please cite this article in press as: D.C. Antonopoulos, V.A. Dougalis. Numerical solution of the 'classical' Boussinesq system, Math. Comput. Simul. (2011), doi:10.1016/j.matcom.2011.09.006

Table 1
Number of solitary waves N that have emerged by $t = 200$ in each wavetrain. CB with $\eta_0(x) = A\exp(-\beta x^2)$, $u_0(x) = 0$.

A	0.3	0.3	0.5	0.5	1.0	1.0	10
β	0.2	0.05	0.2	0.05	0.2	0.05	1/16
N	1	1^+	1	2	1^+	3	8^+

for initial values of the form $\eta_0(x) = A\exp(-\beta x^2)$, $u_0(x) = 0$. (1^+ means that a second solitary wave appears to be in the process of being formed.) The value of N for this type of initial data appears to be proportional to $\int\sqrt{\eta_0}\sim\sqrt{A/\beta}$, reminiscent of the analogous growth of N in the case of the integrable, one-way KdV equation [33]. If SB is integrated with the same initial data, a similar resolution into solitary waves is observed.

As there are no explicit formulas for the solitary waves of CB or SB, highly accurate approximations thereof should be constructed for the purpose of studying their interactions. This may be done by isolating the larger solitary waves produced by long-time simulations of solitary-wave resolution from suitable initial data, after they have separated from the rest of the solution, and then by 'cleaning' them by an iterative process, cf. e.g. [10,20], or by solving numerically two-point boundary-value problems for the second-order o.d.e. in (1.5b) or (1.10b). A detailed study of the accuracy of such procedures has been done elsewhere, cf. e.g. [20], and will not be repeated here. As an example we show in Fig. 3(a) an approximate η-solitary wave of CB that was produced by iterative 'cleaning' after two iterations, starting from an initial profile given by $\eta_0 = 0.3\,\mathrm{sech}^2\left(\sqrt{0.3}(x-50)/2\right)$, $u_0 = 2(\sqrt{\eta_0+1}-1)$ on [0, 600] with $h = 0.1$, $k = 0.01$. The amplitude of the noise behind the wave is of $O(10^{-12})$. The solitary wave that is produced has amplitude 0.423582 and speed 1.18112. Note that if we repeat the 'cleaning' experiment with a finer mesh (cf. Fig. 3(d), obtained with $h = 0.025$, $k = h/10$,) the shelf behind the numerical solitary wave disappears and the noise is reduced to roundoff error level. We have checked that the numerical solitary waves used in the numerical simulations that will be presented in the sequel of this paper propagate, over the temporal intervals of the various experiments, with amplitudes that remain

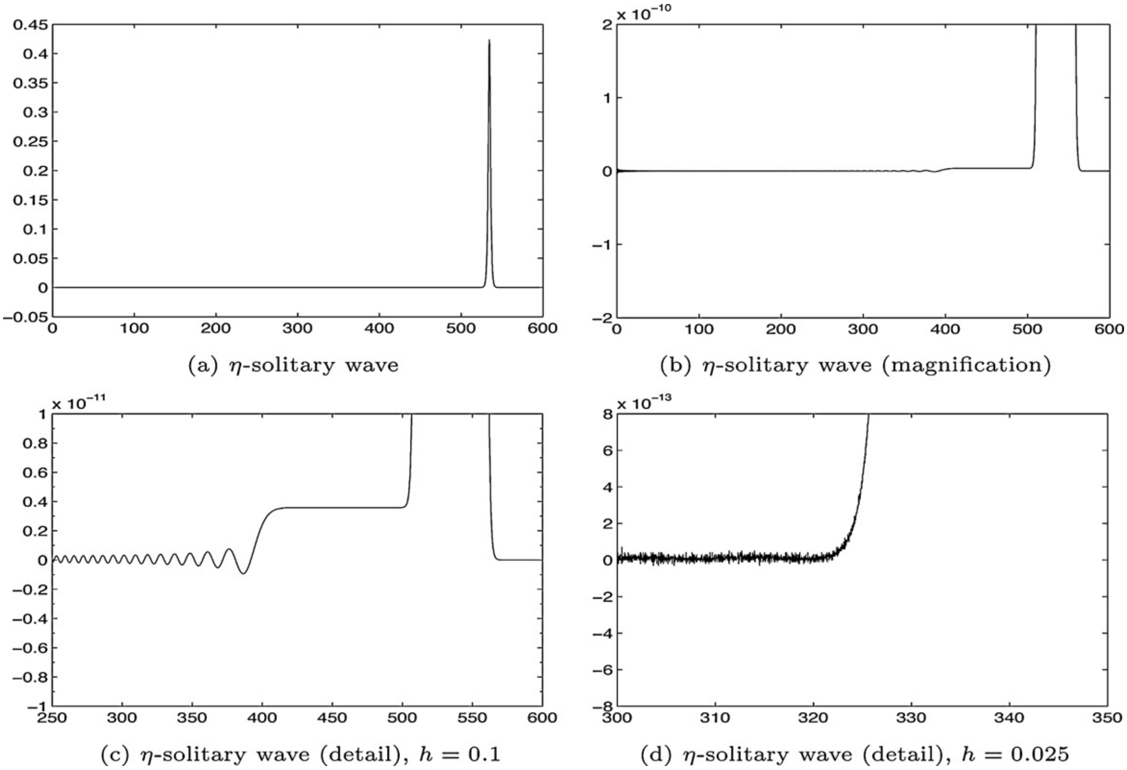

Fig. 3. η-solitary wave of CB produced by iterative 'cleaning' of the larger solitary wave emerging from the evolution of $\eta_0 = 0.3\,\mathrm{sech}^2\left(\sqrt{0.3}(x-50)/2\right)$, $u_0 = 2(\sqrt{\eta_0+1}-1)$.

Table 2
Head-on collision of η-solitary waves, CB and SB systems, →: waves travelling to the right, ←: waves travelling to the left. Shown are the amplitude (A) and speed (c) before and well after the interaction ($t = 150$), the magnitude of the phase shifts of the emerging waves at $t = 150$, and the maximum amplitude of η during the collision.

System	Before				After						Maximum amplitude
	→		←		→			←			
	A	*c*	*A*	*c*	*A*	*c*	*ph.shift*	*A*	*c*	*ph.shift*	
CB	0.801321	1.30567	0.423582	1.18112	0.801211	1.30565	0.3044	0.423604	1.18114	0.3916	1.324023
CB	0.423582	1.18112	Symmetric		0.423577	1.18112	0.3041	Symmetric			0.908484
SB	0.806471	1.40324	0.400551	1.20028	0.806218	1.40309	0.2818	0.400326	1.20016	0.4858	1.331908
SB	0.400551	1.20028	Symmetric		0.400496	1.20025	0.3028	Symmetric			0.866353

constant to six digits and speeds that are constant to five digits, radiate dispersive tails of a maximum amplitude of $O(10^{-10})$, and their (c_s, A_s) values lie exactly on the CB or SB curves of Fig. 1, as the case may be.

3.2. *Head-on collisions of solitary waves.*

Systematic numerical studies of interactions of two solitary waves that travel in opposite directions and collide head-on were performed in the case of Boussinesq systems of the BBM-BBM type in [10] and of the Bona-Smith family in [8], and in the case of the Euler equations in [19]. Here, we would like to point out some features of this type of interaction for solitary waves of the CB and SB systems. All of our experiments were performed on [0, 600] with $h = 0.1$, $k = 0.01$. The initial solitary waves were constructed by iterative ‘cleaning’ with initial η-pulses that were nonnegative and centered sufficiently far from each other, with initial velocity profile of opposite signs.

In our first experiment, a solitary wave of CB with initial η-amplitude $A_1 = 0.801321$ and speed $c_1 = 1.30567$ travels to the right and collides at $t = 50$ with a leftward-travelling solitary wave of initial amplitude $A_2 = 0.423582$ and speed $c_2 = 1.18112$. After they collide, the solitary waves emerge largely unchanged and continue travelling in their respective directions, see Fig. 4(a)–(c). The collision is inelastic, as small-amplitude oscillatory dispersive tails are produced during the interaction and subsequently follow the solitary waves. These dispersive tails are just discernible in Fig. 4(c) and are shown in magnification in (d). They are an integral feature of the interaction and not an artifact of the numerical solution, as they do not change when the computation is repeated with smaller h and k. (The numerical noise level for this experiment stays well below 10^{-10}.) After the interaction, the large solitary wave emerges with a slightly smaller amplitude $A_1{}' = 0.801211$ and speed $c_1{}' = 1.30565$, while the smaller one stabilizes at an amplitude $A_2{}' = 0.423604$ and speed $c_2{}' = 1.18114$. Fig. 4(e) shows the maximum amplitude of η as a function of t for $0 \le t \le 180$. The maximum height that the wave elevation achieves during the collision is equal to 1.324023 which is about 8.1% larger than the sum of the heights of the two solitary waves before the interaction. The temporal transition of the maximum amplitude to its eventual long-time level $A_1{}'$ is non-monotonic, cf. Fig. 4(f). Fig. 4(g) shows the paths of the two solitary waves in the x, t plane around the time of interaction. The solid lines are the actual paths, while the dotted lines represent the paths in the absence of an interaction. Both waves suffer phase shifts opposite to the directions of their motion. At $t = 150$ these shifts are equal to 0.3044 spatial units for the large solitary wave and 0.3916 for the small one. The main quantitative data of this and of subsequent collision experiments are summarized in Table 2. The second line of this table corresponds to the head-on collision of two η-solitary waves of CB of equal heights and opposite speeds. The solitary waves emerge with very slightly smaller amplitudes, the other details of the interaction being analogous to those of Fig. 4. Fig. 5 shows some graphs from the head-on collision of two η-solitary waves of the SB system, whose parameters before and after the interaction are shown in the third line of Table 2. The general picture is similar to that of the analogous interaction in the case of CB, but there are differences such as the larger size of the dispersive tails and the monotonic decrease of the maximum amplitude of the solution to its asymptotic value $A_1{}'$. Finally, the parameters of a head-on collision between η-solitary waves of SB of equal size are shown in the last line of Table 2.

Please cite this article in press as: D.C. Antonopoulos, V.A. Dougalis. Numerical solution of the ‘classical’ Boussinesq system, Math. Comput. Simul. (2011), doi:10.1016/j.matcom.2011.09.006

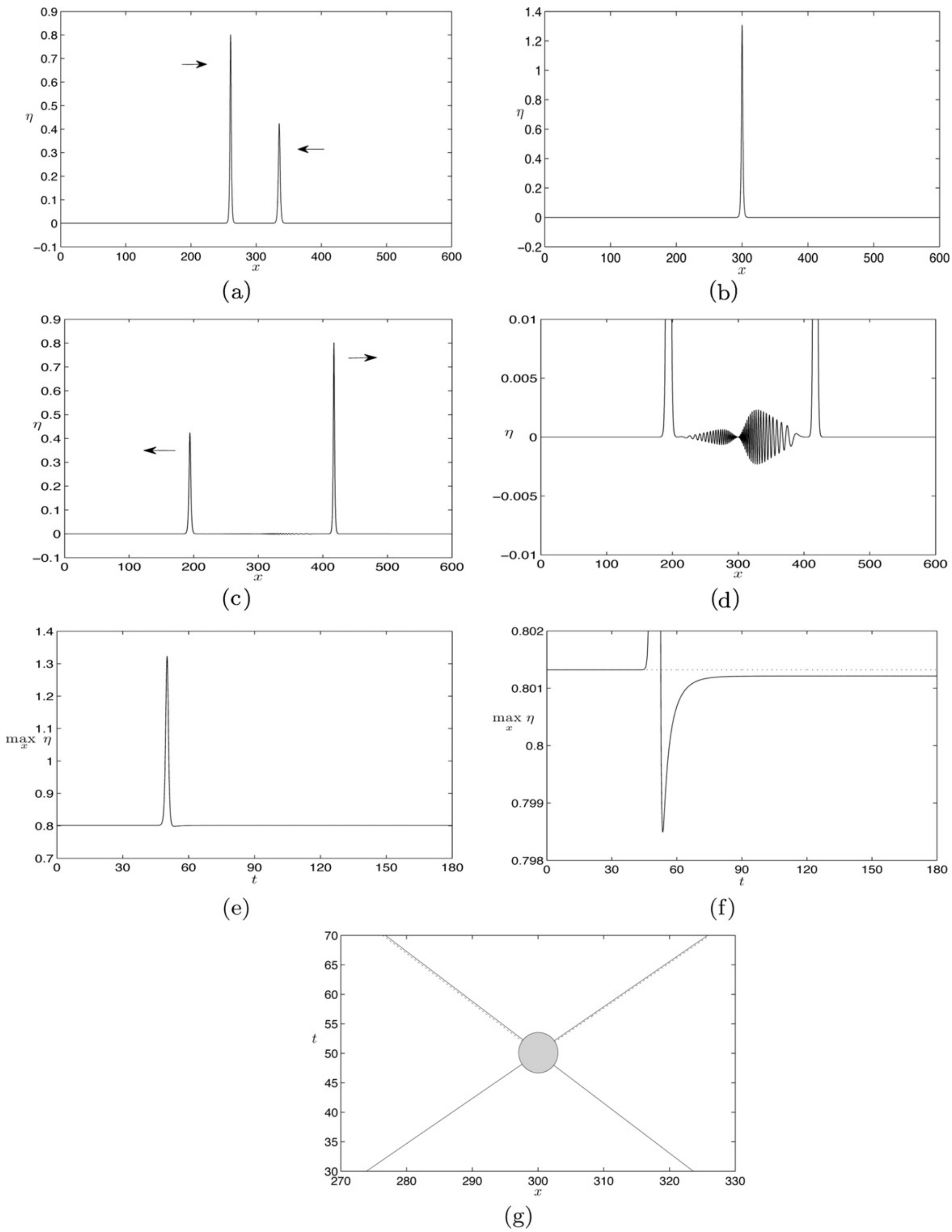

Fig. 4. Head-on collision of two η-solitary waves of CB. (a) $\eta(x, t)$ at $t = 20$, (b) $\eta(x, t)$ at $t = 50$, (c) $\eta(x, t)$ at $t = 140$, (d) dispersive tails, $t = 140$, (e) maximum amplitude of η as a function of t, (f) magnification of (e), (g) paths of the solitary waves in the x,t plane.

Please cite this article in press as: D.C. Antonopoulos, V.A. Dougalis. Numerical solution of the 'classical' Boussinesq system, Math. Comput. Simul. (2011), doi:10.1016/j.matcom.2011.09.006

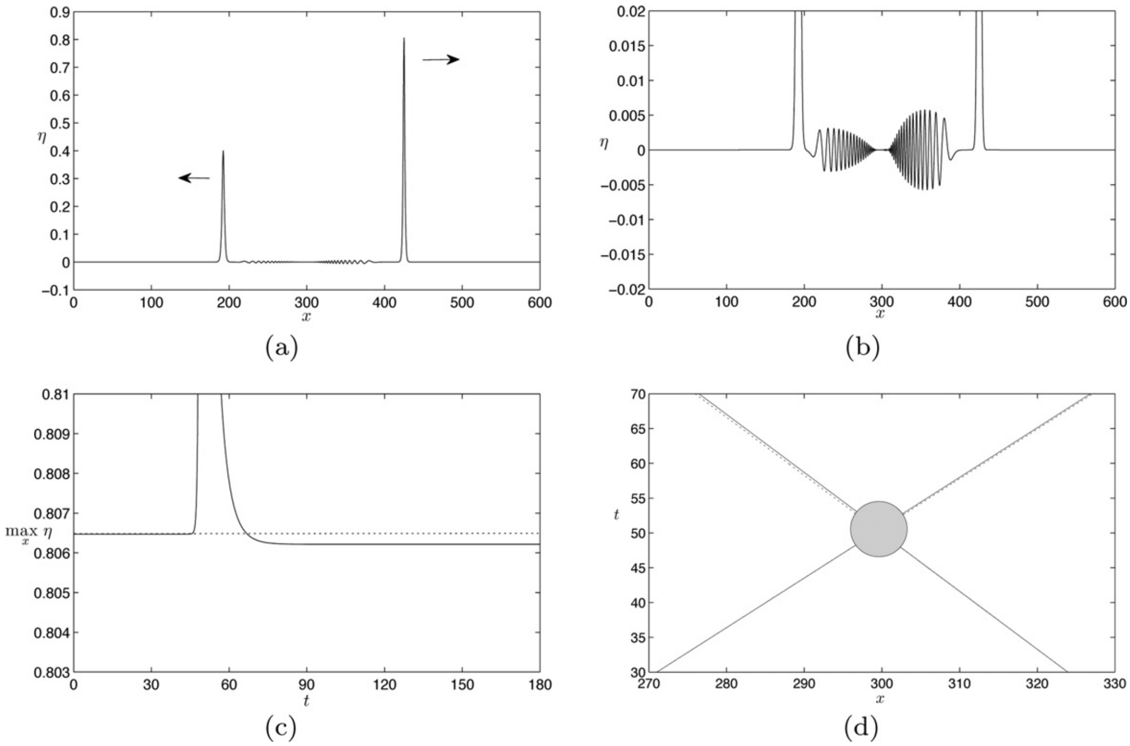

Fig. 5. Head-on collision of two η-solitary waves of SB. (a) $\eta(x, t)$ at $t = 140$, (b) dispersive tails at $t = 140$, (c) magnification of maximum amplitude of η as a function of t, (d) paths of the solitary waves in the x, t plane.

3.3. Overtaking collisions

We describe now *overtaking* collisions of two solitary waves propagating in the same direction. This type of interaction has been studied in depth in the case of one-way models as is well known. See also [8] for a numerical study in the case of Boussinesq systems of the Bona-Smith family and [19] for the Euler equations. The numerical experiments to be described in the sequel were performed on [0, 1200] using periodic boundary conditions and $h = 0.1$, $k = 0.01$.

An overtaking collision of two η-solitary waves of CB is depicted in Fig. 6. Two solitary waves of initial η-amplitudes $A_1 = 0.801321$, $A_2 = 0.423582$, and speeds $c_1 = 1.30567$ and $c_2 = 1.18112$, initially centered at $x = 549.717$ and at $x = 629.658$, respectively, travel to the right, wrap around the boundary at $x = 1200$ due to periodicity, and interact from about $t = 550$ to $t = 700$ as the larger and faster wave overtakes the smaller and slower one. The emerging larger solitary wave has (at $t = 850$) an amplitude $A_1{}' = 0.801320$ and speed $c_1{}' = 1.30565$ while the smaller one has $A_2{}' = 0.423584$, $c_2{}' = 1.18115$. Fig. 7 shows several instances of the overtaking interaction (with the x-axis much magnified) in the temporal interval $605 \leq t \leq 620$. We observe that the two peaks are always present, one diminishing and the other growing; they become equal in height attaining a common value of 0.573604 at $t = 614.3$. (Contrast this to the case of head-on collision, where the two interacting solitary waves momentarily merge into a single pulse, cf. Fig. 4(b).) Note that the minimum amplitude during the interaction stays above the height of the smaller solitary wave. (Fig. 8(b) shows the graph of $\max_x \eta(x, t)$ as a function of time for $0 \leq t \leq 900$.)

Both waves undergo phase changes during the interaction, cf. Fig. 8(a): The larger wave is pushed forward while the smaller one is delayed. The overtaking collision is inelastic. As depicted in the plots of Fig. 9, which show details of the solution towards the end of the interaction with the η-axis much magnified, two types of dispersive small-amplitude oscillations are produced: A dispersive tail of small wavelength, decaying oscillations that travel to the right following the solitary waves, and a N-shaped ‘wavelet’ of very large wavelength and small amplitude that travels to the left. This picture is in good qualitative agreement with analogous observations in [19,8], in the context of the Euler equations and the Bona-Smith Boussinesq systems, respectively. (The ‘wavelet’ was first identified by Su and Zou [32], in the course

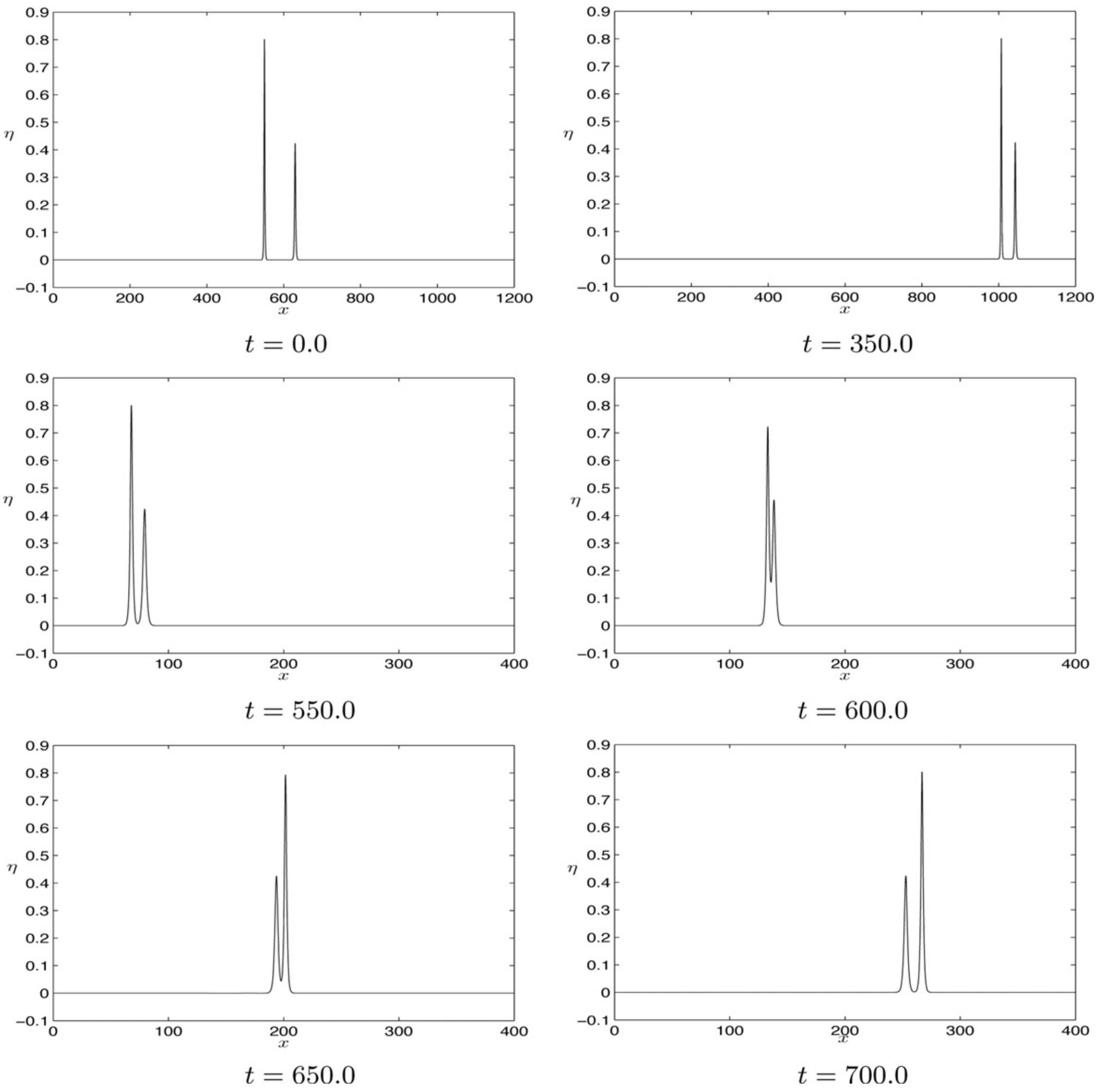

Fig. 6. Overtaking collision of two η-solitary waves of CB.

of their investigation of overtaking collisions of solitary waves of the Euler equations. Their numerical model was based on a single, Boussinesq-type equation with an ∂_{xxtt} fourth-order term, which is derived from CB under a one-way assumption.) As the plots in Fig. 10 show, the wavelet is dispersive. At the time instance $t = 900$ of the evolution shown in Fig. 9, the time clock is set to zero and the wavelet is cut off the rest of the solution (which is set equal to zero in the interval [244.3, 675]) and left to propagate to the left. At $t = 700$, the profile of the wavelet is shown in Fig. 10(a). As the wavelet moves, its shape and speed are slowly changing: Fig. 10(b) shows that the amplitude of its positive (+) peak is decreasing, while the absolute amplitude of the negative (−) peak is increasing with time. While Fig. 10(c), that depicts the paths of the two peaks in the t, x plane, would seem to suggest that the speeds of the peaks are equal and constant, actually this is not the case in view of Fig. 10(d) in which the distance of the two paths is seen to be slowly increasing.

The details of the overtaking collision of two solitary waves of the SB system are qualitatively the same. For initial solitary waves of the same magnitude, the sizes of the dispersive tail and of the wavelet are about double those of the analogous quantities of the CB.

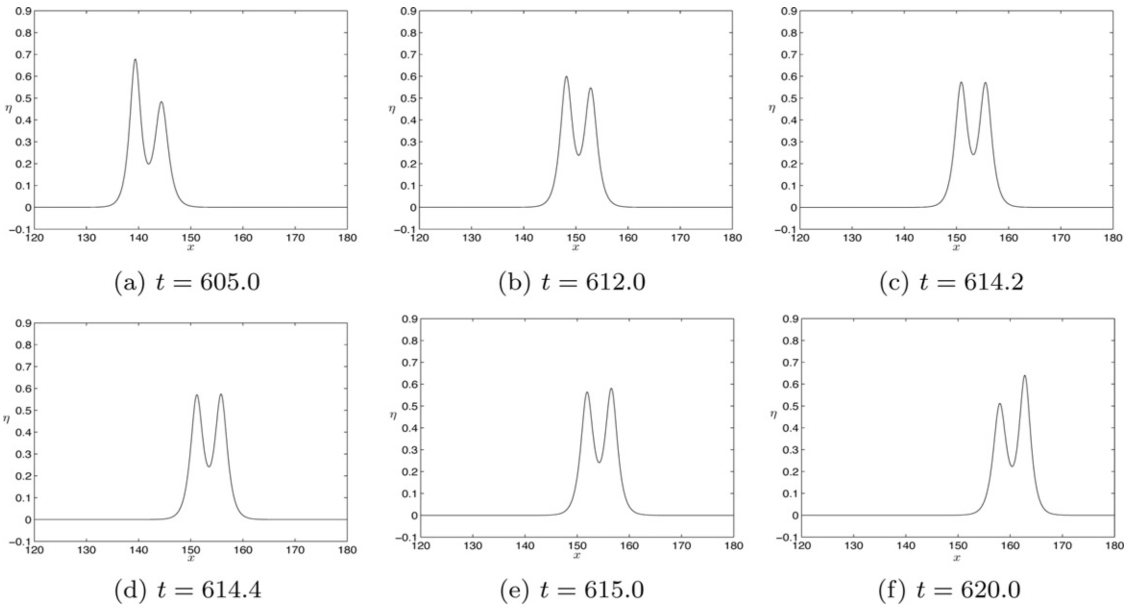

Fig. 7. Details of the overtaking collision of two η-solitary waves of CB of Fig. 6.

3.4. Interaction of solitary waves with the boundary

When a solitary wave of the CB or the SB systems hits a boundary point at which the condition $u = 0$ has been prescribed, it is observed that the wave is reflected backwards while a dispersive tail is formed and follows the reflected wave. This is illustrated in Fig. 11, wherein the solitary wave produced by iterative cleaning, as described in Section 3.1, and whose η-component is shown in Fig. 3, has travelled to the right, hit the boundary at $x = 600$ at about $t = 455$, has been reflected backwards, and is observed travelling to the left, followed by a dispersive tail in the pairs of Fig. 11(a) and (b), and (c) and (d), at $t = 500$ and $t = 550$, respectively. In Fig. 11(e) we plot $\max_x \eta(x, t)$ and observe in (f) that the reflected pulse after a momentary dip regains an amplitude which stabilizes eventually to the value 0.423577. The paths of the incident and the reflected wave in the x, t plane are shown in Fig. 11(g) (note the delay during the interaction at the boundary), while Fig. 11(h) shows the graph of the speed of the pulse as a function of time (with negative values for the reflected wave). The speed of the reflected pulse stabilizes to a value that is measured to be equal to 1.81112 in absolute value. Thus, it is apparent that the incident solitary wave is reflected backwards forming a new, slightly smaller solitary wave which is followed by a dispersive tail. An analogous experiment with the symmetric system SB shows that an incident solitary wave of η-amplitude 0.400551 and speed 1.20028 produces a reflected solitary wave

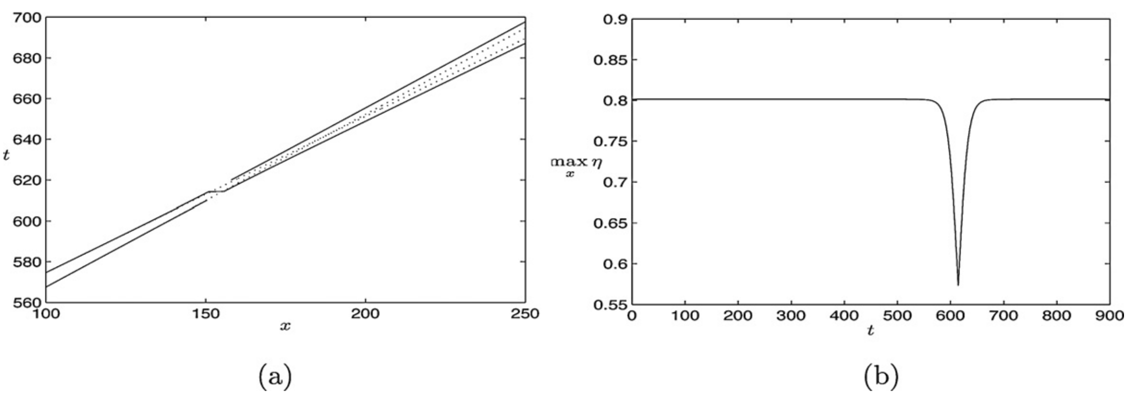

Fig. 8. Overtaking collision of Fig. 6: (a) paths of the solitary waves in the x,t plane, (b) $\max_x \eta(x, t)$.

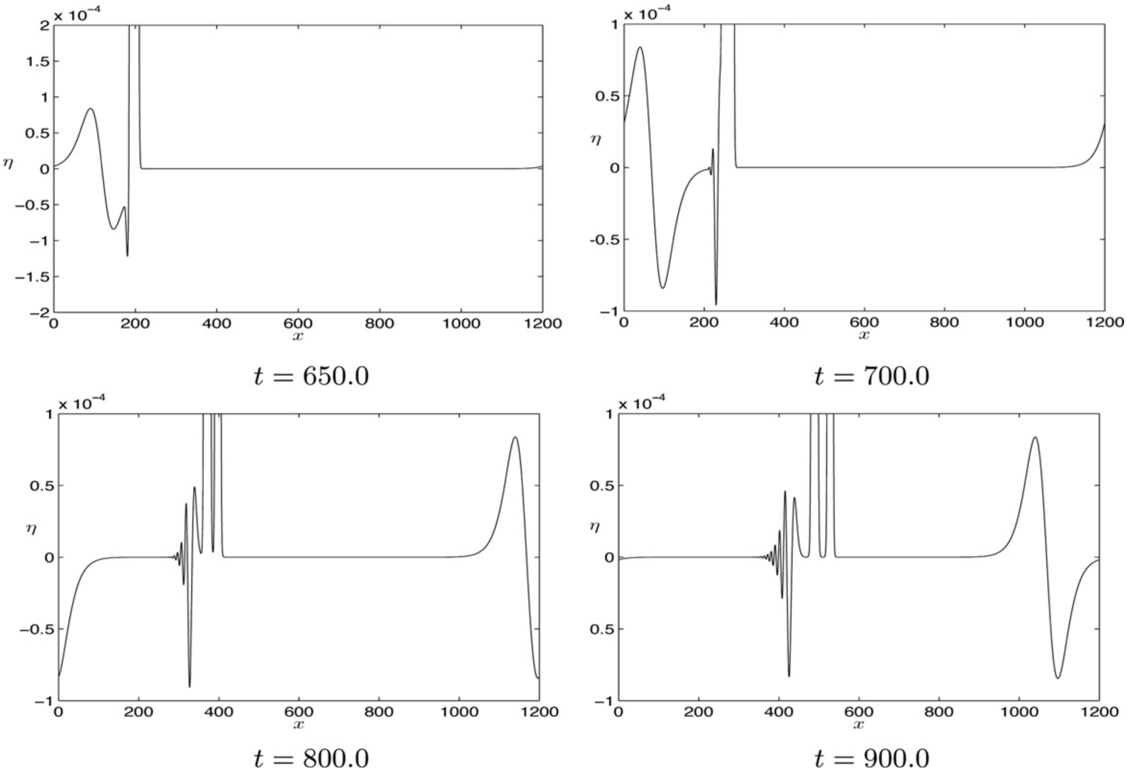

Fig. 9. Dispersive tail and wavelet produced during the overtaking collision of Fig. 6.

whose amplitude monotonically decreases to 0.400496 and whose speed in absolute value is 1.20025. The dispersive oscillations are now of larger amplitude.

In the case of ideal fluids, the normal reflection of a solitary wave of elevation from a wall is equivalent to (one-half) of the head-on collision of the solitary wave with its image of equal height and opposite velocity, provided there is no loss of symmetry in the latter interaction [17]. This equivalence has been observed in numerical simulations of solitary wave interactions of one-dimensional models for two-way long wave propagation, for example in the case of the Bona-Smith family of Boussinesq systems [8]. The wall reflection boundary conditions for that family of systems are $\eta_x = 0$ and $u = 0$. By symmetry, these conditions hold at the center of the head-on collision of two solitary waves of equal height; one cannot observe any differences in the numerical simulations of a reflected solitary wave and the wave emerging from a head-on collision with its image.

In the case of the CB or the SB system at hand, the boundary condition that is sufficient for well-posedness (and is imposed by the numerical scheme) is just $u = 0$. On the other hand, we expect that at the center of the head-on collision we will have $u = 0$ and $\eta_x = 0$. The question arises whether $\eta_x = 0$ holds at the reflection boundary.

We investigate this problem numerically in the case of the CB system. In Fig. 12(a), we show, in magnified form near the boundary point $x = 300$, where $u = 0$ is prescribed, the base of the reflected η-solitary wave and the trailing dispersive tail at $t = 73.25$. (Initially, the solitary wave was the one produced by iterative cleaning and shown in Fig. 3. Centered initially at approximately $x = 234.62$, it travels to the right and starts to interact with the wall at about $t = 50$. The computation of the evolution shown in Fig. 12 was done on [0, 300] with $h = 0.05$, $k = h/10$.) On this reflected profile we have superimposed another curve, the numerical approximation of the leftward-travelling wave emerging from the head-on collision of the initial solitary wave with its symmetric (with respect to $x = 300$) image of opposite velocity, initially located outside the domain. There is no observed difference within graph thickness, and this persists (cf. Fig. 12(b) and (d)) to at least $t = 175$ when the run was terminated. (Note the change of vertical scale in Fig. 12(c) and (d).)

In order to investigate matters more closely we computed η_x at $x = 300$ as a function of t for the reflected wave and the wave emerging from the head-on collision. The results are shown in Fig. 13. The left-hand side graph depicts the

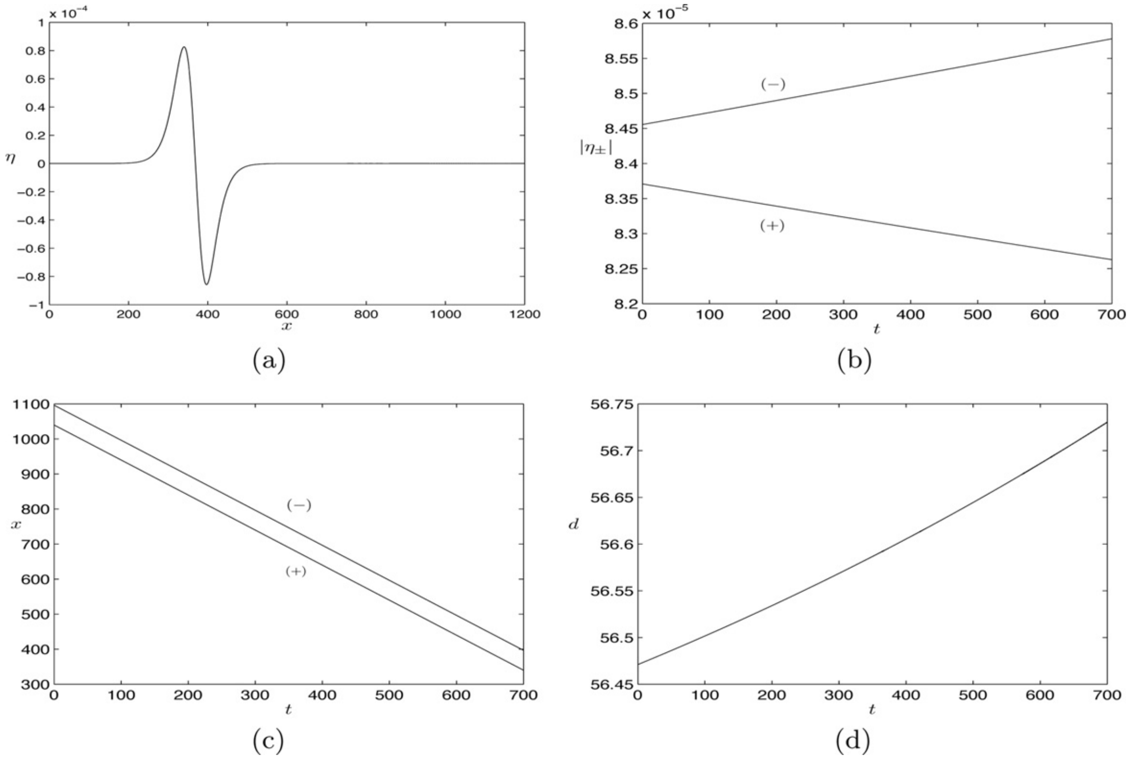

Fig. 10. Wavelet produced by the overtaking collision of Figs. 6 and 9. (a) Wavelet at $t = 700$ after its cleaning, (b) absolute value of the peaks of the wavelet as function of t, (c) paths of the peaks in the t, x plane, (d) distance of peaks as function of t.

function $\eta_x(300, t)$ for $0 \leq t \leq 150$ for the solitary wave emerging from the head-on collision with center at $x = 300$. As expected, due to the symmetry of the interaction, its magnitude is very small (of $O(10^{-13})$). On the other hand, the order of magnitude of the amplitude of the same function (right-hand graph of Fig. 13) for the reflected wave is of $O(10^{-6})$. We computed the quantity $\eta_x(300, t)$ for the reflected wave at various values of t as a function of diminishing h (with $k = h/10$) and obtained the results shown for $t = 55$ and $t = 100$ in Table 3. (The computation for $h = 0.025$ on [0, 300], which includes the iterative cleaning of the initial solitary wave, is very hard and time consuming.) As $h \downarrow 0$ it appears that approximately $|\eta_x(300)| = O(h^3)$ for all values of t that we tested. (Note that the expected order of magnitude of the $W^{1,\infty}$ error of the Galerkin method with cubic splines for this problem is $O(h^2)$. Hence, we have here a superaccuracy phenomenon.) We conclude that although the numerical scheme does not satisfy the condition $\eta_x = 0$ at the wall, it is able to sense that the reflected wave has this property and it approximates it well as $h \downarrow 0$.

We should of course add that all this discussion pertains to reflection of solitary-wave like pulses. For other types of initial profiles satisfying $\eta_x = 0$ and $u = 0$ at the boundaries, only the imposed boundary condition $u = 0$ persists for $t > 0$.

Table 3
$|\eta_x(300, t)|$ at $t = 55$ and $t = 100$ as $h \downarrow 0$, CB.

h	$t = 55$		$t = 100$	
	$\|\eta_x(300)\|$	Order	$\|\eta_x(300)\|$	Order
0.1	4.98693(−5)		1.50532(−5)	
0.05	6.28694(−6)	2.988	1.96258(−6)	2.939
0.025	7.87455(−7)	2.997	2.50019(−7)	2.973

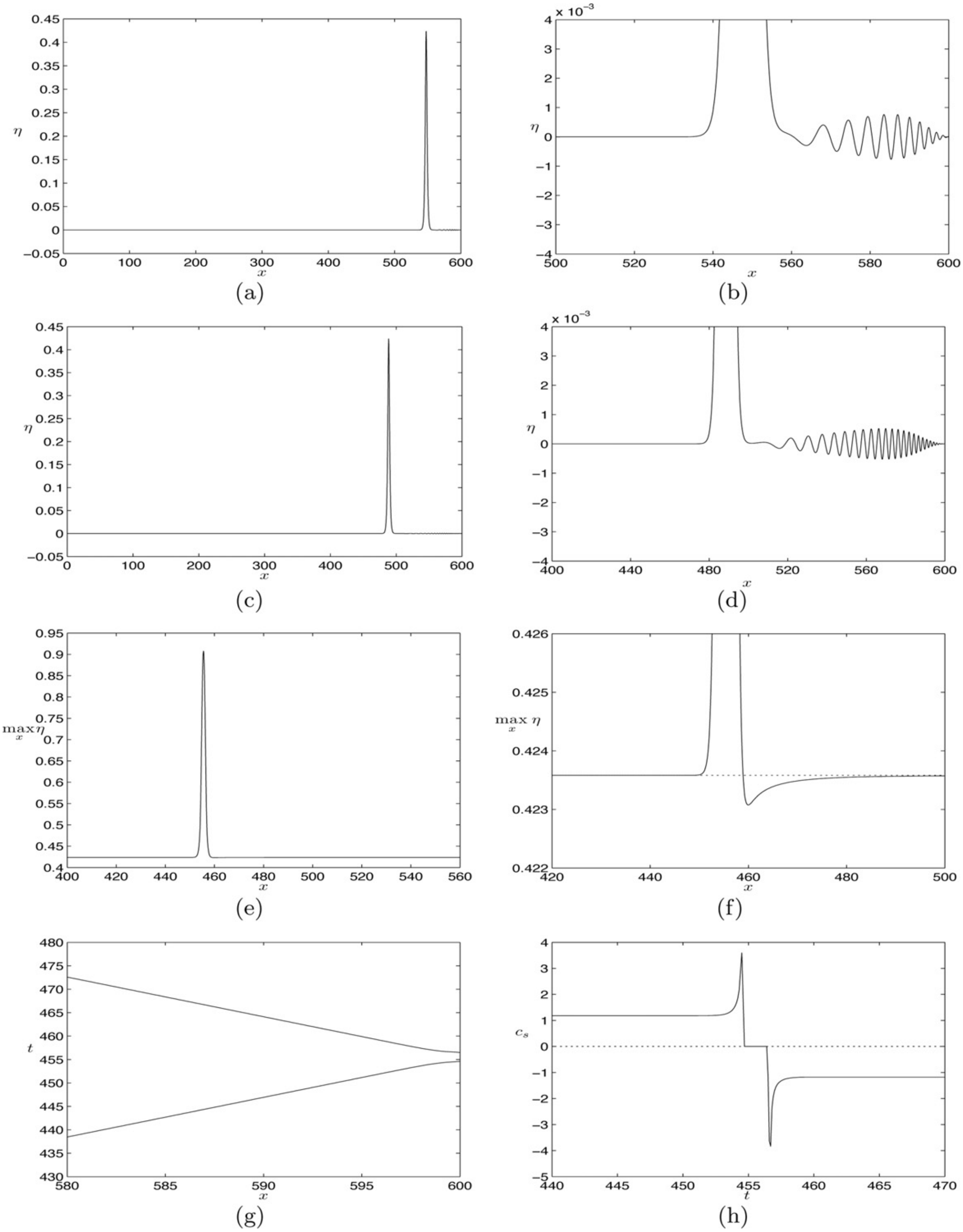

Fig. 11. Interaction of a CB solitary wave with the boundary at $x = 600$. (η-profiles) (a) The reflected wave at $t = 500$, (b) magnification of (a), (c) reflected wave at $t = 550$, (d) magnification of (c), (e) $\max_x \eta(x, t)$, (f) magnification of (e), (g) paths of incident and reflected wave in the x, t plane, (h) speed c_s as a function of time.

Please cite this article in press as: D.C. Antonopoulos, V.A. Dougalis. Numerical solution of the 'classical' Boussinesq system, Math. Comput. Simul. (2011), doi:10.1016/j.matcom.2011.09.006

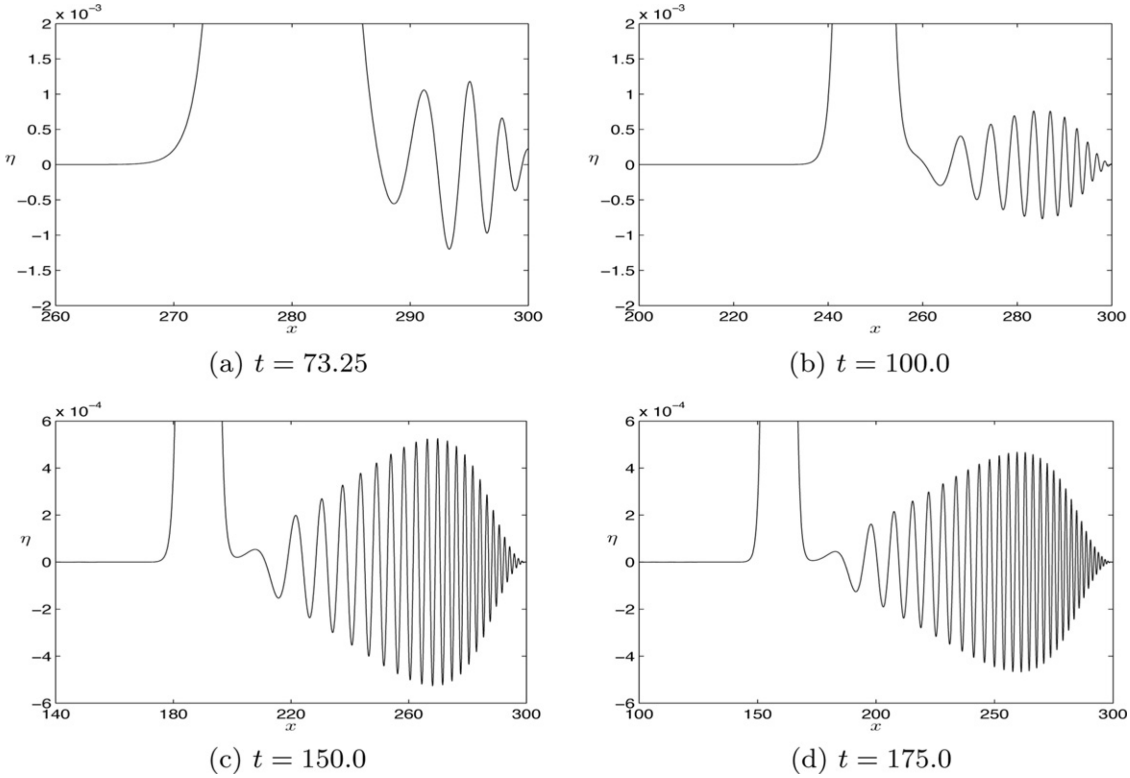

Fig. 12. Reflected η-solitary wave from the wall at $x = 300$ (where $u = 0$) superimposed on one half of the wave emerging from the associated head-on collision. CB system.

3.5. Blow-up of solutions in finite time

We observed that numerical solutions of the ibvp's (2.1) or (2.2) may apparently blow up in finite time when the initial data are suitably large. (In contrast with the global well-posedness theory of the Cauchy problem for the CB system, wherein suitable decay conditions at infinity on the initial data ensure existence and uniqueness of smooth solutions for all $t > 0$, the existing well-posedness theory for the ibvp (2.1) [1], does not preclude possible loss of regularity of solutions in finite time.) This is illustrated in Fig. 14. The ibvp (2.1) is integrated numerically on the spatial interval [0, 1] with $h = 10^{-3}$, $k = h/10$, and initial conditions $\eta_0(x) = 0.9\sin(2\pi x)$, $u_0(x) = 5x(x-1)$, $0 \le x \le 1$. The large, negative initial velocity imparted to the wave pushes it to the left boundary, where it is reflected rightwards

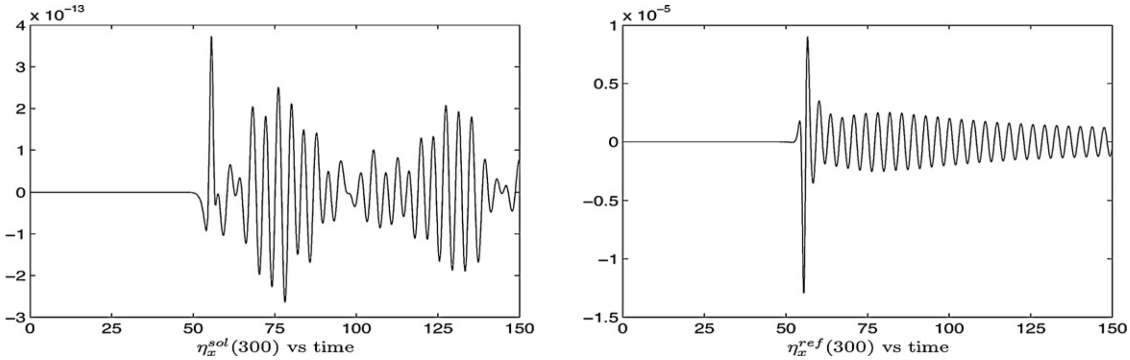

Fig. 13. The function $\eta_x(300, t)$ for $0 \le t \le 150$ for the reflected solitary wave (right) and the wave emerging from the head-on collision (left). Evolution of Fig. 12.

Please cite this article in press as: D.C. Antonopoulos, V.A. Dougalis. Numerical solution of the 'classical' Boussinesq system, Math. Comput. Simul. (2011), doi:10.1016/j.matcom.2011.09.006

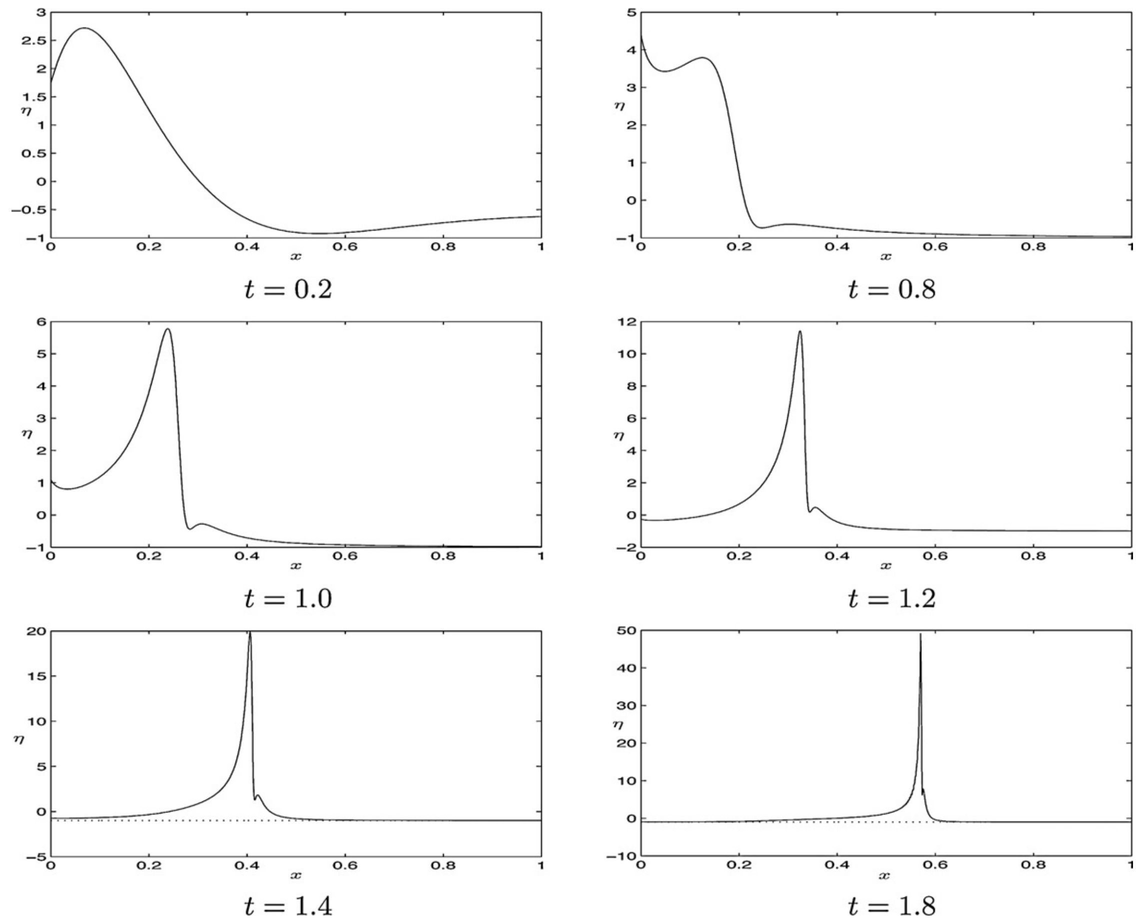

Fig. 14. Apparent finite-time blow-up of solutions of ibvp (2.1) for CB, η-profiles.

(Fig. 14, $t = 0.2$, 0.8). The elevation η of the wave then forms a peak that develops into a thin spike which apparently increases without bound in height. Loss of numerical accuracy occurred shortly after $t = 1.8$. It is worthwhile to note that the velocity u does not blow up; it remains bounded, apparently tending to form a discontinuity in u_x as the blow-up point is approached. (Cf. Fig. 15 for the final stages of the u-profile.) This is consistent with the theory in [1] which ensures that u remains in $H_0^1(0, L)$.

While, of course, one cannot be absolutely certain about blow-up based on numerical evidence, we are fairly confident that blow-up occurs in this example. When the experiment was repeated with smaller h and k the thin spike

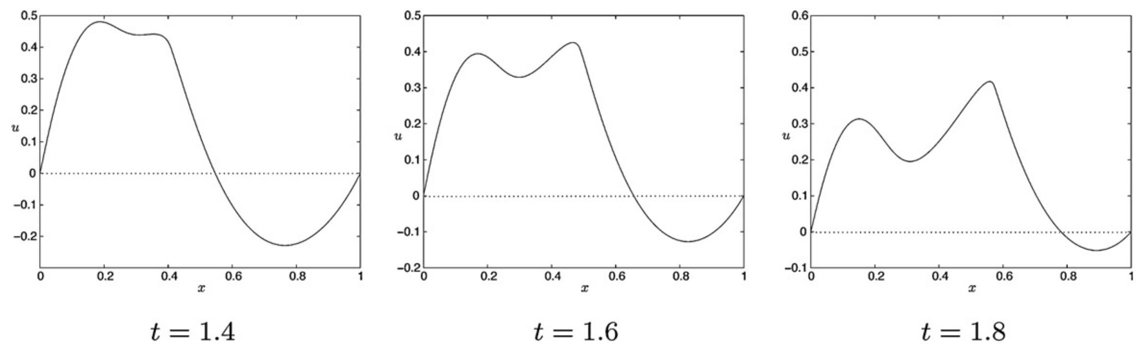

Fig. 15. Velocity profiles of the evolution of Fig. 14 as blow-up is approached.

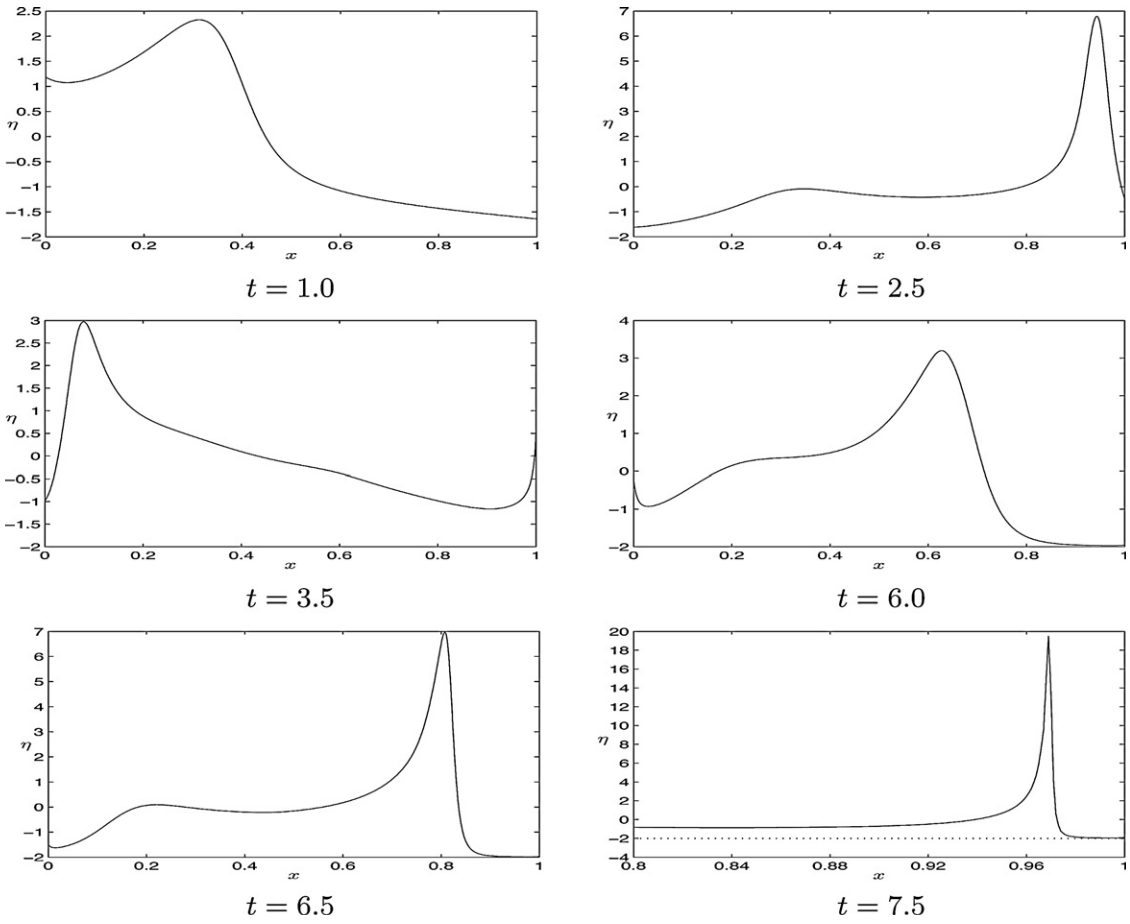

Fig. 16. Apparent finite-time blow-up of solutions of ibvp (2.2) for SB, η-profiles.

was formed at approximately the same 'blow-up' point (x^*, t^*). A full numerical study of the blow-up requires a space – and time – adaptive code for dynamic mesh refinement as (x^*, t^*) is approached, in the spirit e.g. of [14], and is outside the scope of the present note.

A few remarks are in order. In the case of other Boussinesq systems, for example of the Bona-Smith systems, cf. [20], it was observed that the solution evolving from initial conditions that were suitable large perturbations of solitary waves of these systems produced nonphysical η-profiles with values less than the bottom level -1. Such solutions typically blew up soon after. The mode of blow-up that we observe here is different. The η-component of the solution always stays above -1 and the total mass $\int_0^1 \eta\, dx$ is conserved, in the case of both the continuous problem (2.1) and its semidiscrete analog. (Note that in the case of the Cauchy problem for CB, cf. [30], a maximum principle argument for the parabolic regularization of the first p.d.e. of (1.1) with a term $\mu\eta_{xx}$ in its right-hand side ensures that $1+\eta^{\mu}(x, t) \geq 0$ for $x \in \mathbb{R}$, $t \geq 0$ and all $\mu > 0$, where η^{μ} is the classical solution of the regularized system, evolving from suitably smooth initial data such that $\eta_0(x) > -1$, $x \in \mathbb{R}$. Our numerical examples suggest that this property is inherited by smooth solutions of the ibvp (2.1) as well.)

When the ibvp (2.2) for the SB system is integrated in time with the same initial conditions and numerical parameters as in the previous example, one obtains the evolution whose η-component is depicted at several temporal instances in Fig. 16. Now the wave that is reflected from the left-hand boundary $x = 0$ travels to the right, is reflected backwards and forwards again before forming the peak at about $t = 6$ that subsequently develops into a thin spike that apparently blows up at about $t = 7.5$. Again, the velocity u remains bounded and apparently develops a discontinuity in u_x as the blow-up point is approached, exactly as in the case of CB. (The conservation property (1.9) does not preclude a point blow-up in η but ensures that u remains in $H_0^1(0, L)$. In the semidiscrete approximation (1.9) still holds, with (η_h, u_h)

Please cite this article in press as: D.C. Antonopoulos, V.A. Dougalis. Numerical solution of the 'classical' Boussinesq system, Math. Comput. Simul. (2011), doi:10.1016/j.matcom.2011.09.006

Table 4
$E_s(t)$ for $s=0$ (L^2-error) and for $s=1$ (H^1-error) for CB initial data (3.6) at $t=1, 2, 10, 20$ as $\varepsilon \downarrow 0$, and its order as a function of ε.

Time	1.0		2.0		10.0		20.0	
ε	L^2-error	Order	L^2-error	Order	L^2-error	Order	L^2-error	Order
10^{-2}	2.8114(−05)		5.1767(−05)		1.8564(−04)		2.0708(−04)	
10^{-3}	3.4124(−07)	1.916	6.8149(−07)	1.881	3.1003(−06)	1.777	5.7951(−06)	1.553
10^{-4}	3.7392(−09)	1.960	7.6778(−09)	1.948	3.6557(−08)	1.928	7.1190(−08)	1.911
10^{-5}	3.6917(−11)	2.006	7.7543(−11)	1.996	4.0391(−10)	1.957	7.8851(−10)	1.956

Time	1.0		2.0		10.0		20.0	
ε	H^1-error	Order	H^1-error	Order	H^1-error	Order	H^1-error	Order
10^{-2}	2.2014(−04)		3.4608(−04)		1.0821(−03)		8.1559(−04)	
10^{-3}	5.2060(−06)	1.626	8.9329(−06)	1.588	2.5358(−05)	1.630	4.0541(−05)	1.304
10^{-4}	1.6721(−07)	1.493	3.2340(−07)	1.441	7.1724(−07)	1.548	1.1570(−06)	1.545
10^{-5}	2.5158(−09)	1.823	6.0466(−09)	1.729	2.5913(−08)	1.442	3.7040(−08)	1.495

replacing (η, u), and implies that $\|u_h\|_\infty$ can be bounded independently of h.) Note that the temporal span of existence of this SB solution is larger than that of its CB analog and that the solution persists well past the temporal instance (at about $t=0.1$) when η first dips below the bottom level at -1 and enters a nonphysical regime. As in the CB case, the total mass is conserved. In addition, up to blow-up we observe that $\eta \geq -2$, something that could be explained again from a maximum principle argument for the parabolic regularization of the first p.d.e. of SB which is easily seen to satisfy $2+\eta^\mu \geq 0$ provided $2+\eta_0>0$.

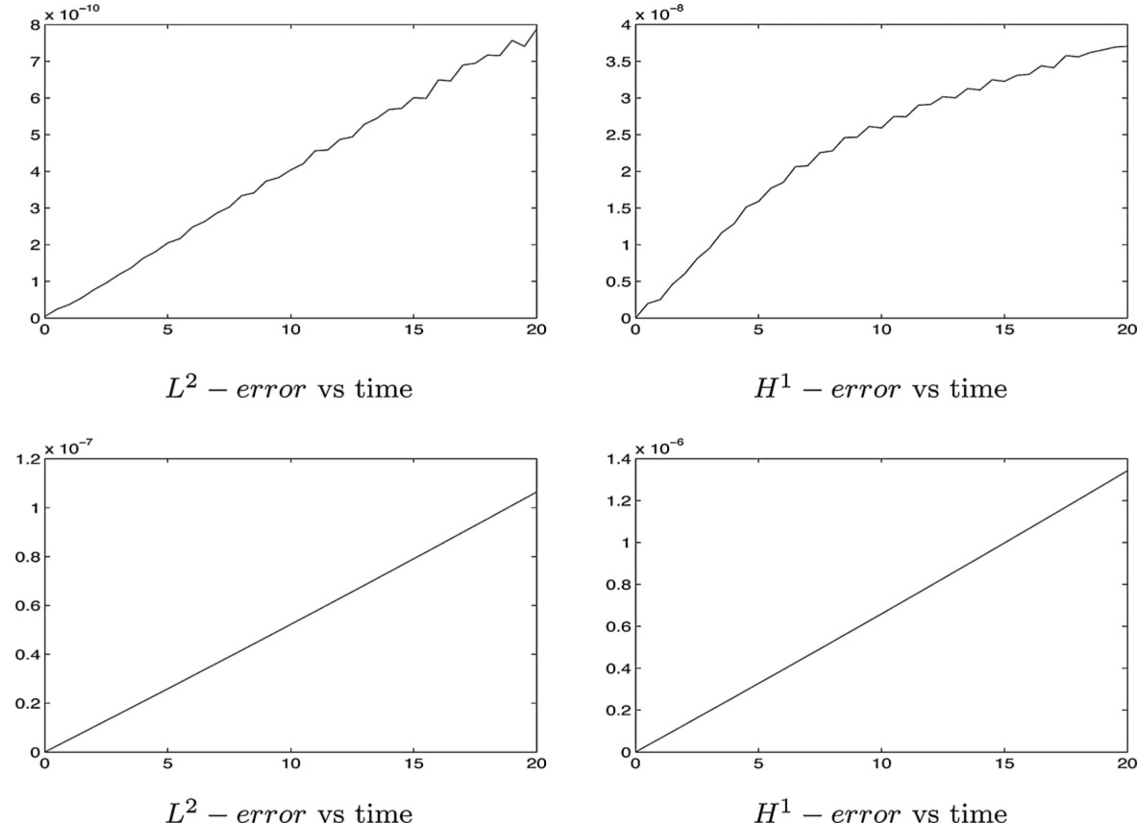

Fig. 17. L^2- and H^1-errors as functions of $t \in [0, 20]$ for $\varepsilon = 10^{-5}$ for CB initial conditions (3.6) (upper figures) and (3.7) (lower figures).

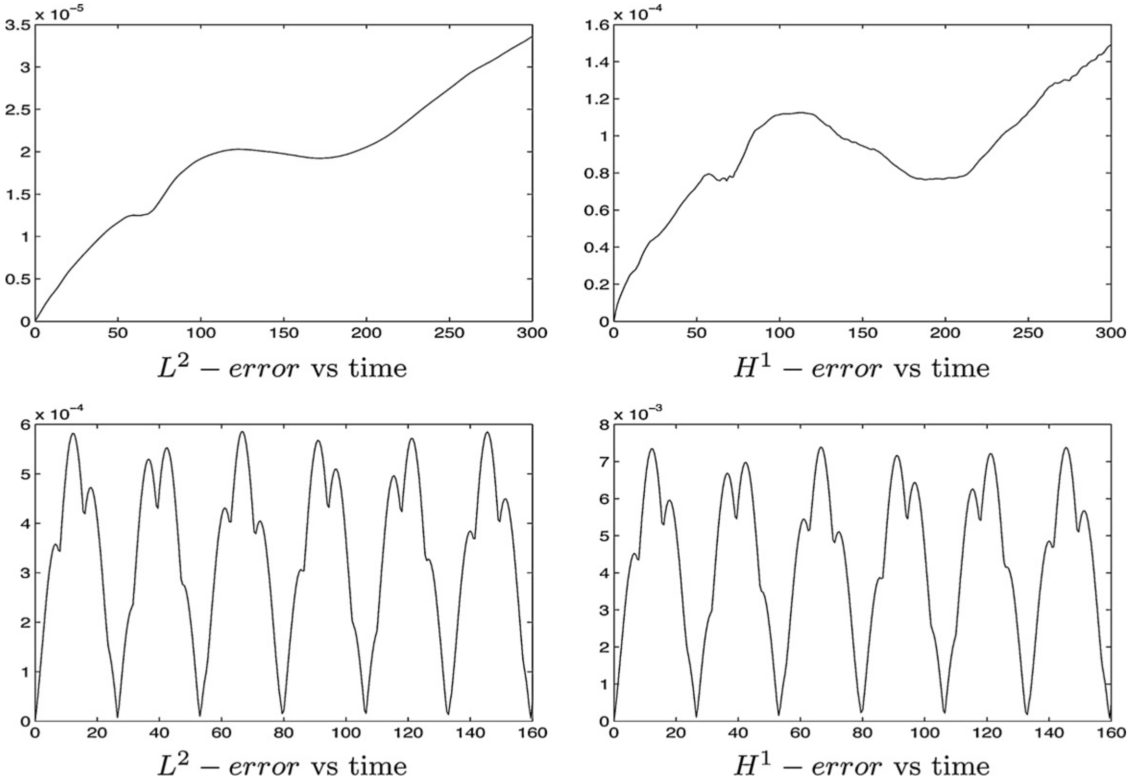

Fig. 18. L^2- and H^1-errors as functions of t for $\varepsilon = 10^{-3}$ and for longer temporal intervals given CB initial conditions (3.6) (upper figures), and (3.7) (lower figures).

3.6. Comparison of solutions of CB and SB in scaled form.

In this section we shall compare solutions of the two systems CB and SB in their scaled forms (1.4) and (1.8), respectively, for small values of the parameter ε. In the sequel we shall denote solutions of the ibvp for the scaled CB as $(\eta^\varepsilon, u^\varepsilon)$ and of the scaled SB system as $(\eta_\Sigma^\varepsilon, u_\Sigma^\varepsilon)$.

In the case of the *Cauchy problem* for the systems, it may be inferred from [13,2], in view of the global existence and uniqueness results for CB, that if the initial data for the two systems are smooth, decay fast enough at infinity and are related by the formulas

$$\eta_{0,\Sigma}^\varepsilon = \eta_0^\varepsilon, \quad u_{0,\Sigma}^\varepsilon = u_0^\varepsilon\left(1 + \frac{\varepsilon}{2}\eta_0^\varepsilon\right), \tag{3.4}$$

then, at least on temporal intervals of the form $[0, T_\varepsilon]$, where $T_\varepsilon = O(1/\varepsilon)$, we have, e.g. for $s = 0$ and 1, that for ε small enough

$$\|\eta^\varepsilon - \eta_\Sigma^\varepsilon\|_{L^\infty(0,t;H^s)} + \left\|u^\varepsilon - u_\Sigma^\varepsilon\left(1 - \frac{\varepsilon}{2}\eta_\Sigma^\varepsilon\right)\right\|_{L^\infty(0,t;H^s)} \le C\varepsilon^2 t \quad \text{for } t \in [0, T_\varepsilon], \tag{3.5}$$

where $H^s = H^s(\mathbb{R})$ and C is a constant independent of ε and t.

In what follows our goal is to investigate numerically whether an inequality of the type (3.5) holds, given initial data that satisfy (3.4), when the systems are posed as ibvp's on the fixed spatial interval [0, 1] at the endpoints of which it is assumed, as usual, that the velocity variable is zero. In all numerical experiments we discretized the problems with $h = 0.01$, $k = 0.001$. In our first experiment we took as initial data for CB the functions

$$\eta_0^\varepsilon = 1, \qquad u_0^\varepsilon = x(x-1), \quad 0 \le x \le 1, \tag{3.6}$$

and compared the solution of the ibvp of CB to that of SB at several fixed values of $t \in [0, 20]$ as $\varepsilon \downarrow 0$, by computing the quantity

$$E_s(t) = \|\eta^\varepsilon - \eta_\Sigma^\varepsilon\|_s + \left\| u^\varepsilon - u_\Sigma^\varepsilon \left(1 - \frac{\varepsilon}{2}\eta_\Sigma^\varepsilon\right) \right\|_s,$$

that will subsequently be referred to as 'L^2-error' when $s = 0$ and as 'H^1-error' when $s = 1$. We then estimated its 'order' α by assuming that $E_s = O(\varepsilon^\alpha)$. Numerical results such as those shown in Table 4 suggest that as $\varepsilon \downarrow 0$ $E_0(t)$ is very close to $O(\varepsilon^2)$ for all $t \in [0, 20]$, while $E_1(t)$ seems to stabilize to $O(\varepsilon^{1.5})$. In the case of the CB initial data

$$\eta_0^\varepsilon = \cos(2\pi x), \qquad u_0^\varepsilon = \sin(2\pi x), \quad 0 \le x \le 1, \tag{3.7}$$

that has a smooth periodic extension to $(-\infty, \infty)$, the analogous numerical experiment gives that $E_s(t) = O(\varepsilon^2)$ for $t \in [0, 20]$ for $s = 0$ and $s = 1$. For both sets of initial data and for small ε, the initial temporal dependence of $E_s(t)$ is very close to linear, as Fig. 17 suggests. Our conclusion is that in the case of the type of ibvp's for CB and SB that we considered, a result like (3.5) apparently holds for small enough t in the case $s = 0$, while there might be initial data for which the exponent of ε in the right hand side is less than 2 if $s = 1$. We subsequently took a fixed value of $\varepsilon = 10^{-3}$ and computed the quantities $E_s(t)$ for $s = 0, 1$ for longer temporal intervals over which the ibvp's of both systems apparently had bounded solutions. In the case of CB initial conditions (3.6), Fig. 18 suggests that $E_s(t)$ for $s = 0, 1$ is initially and eventually increasing with t, for $t \in [0, 300]$, roughly linearly. For the periodic CB initial data (3.7) $E_s(t)$ exhibits *grosso modo* a periodic-like temporal behavior.

References

[1] K. Adamy, Existence of solutions for a Boussinesq system on the half line and on a finite interval, Discrete Continuous Dynamical Syst. A 29 (2011) 25–49.
[2] B. Alvarez-Samaniego, D. Lannes, Large time existence for 3D water-waves and asymptotics, Invent. Math. 171 (2008) 485–541.
[3] C.J. Amick, Regularity and uniqueness of solutions to the Boussinesq system of equations, J. Diff. Eqns. 54 (1984) 231–247.
[4] D.C. Antonopoulos, The Boussinesq system of equations: theory and numerical analysis, Ph.D. Thesis, University of Athens, 2000 (in Greek).
[5] D.C. Antonopoulos, V.A. Dougalis, Numerical approximations of Boussinesq systems, in: A. Bermudez, et al. (Eds.), Proceedings of the 5th International Conference on Mathematical and Numerical Aspects of Wave Propagation, SIAM, Philadelphia, 2000, pp. 265–269.
[6] D.C. Antonopoulos, V.A. Dougalis, Galerkin methods for the Bona-Smith version of the Boussinesq equations, in: P.S. Theocharis, et al. (Eds.), Proceedings of the 5th National Congress on Mechanics, Ioannina, 1998, pp. 1001–1008.
[7] D.C. Antonopoulos, V.A. Dougalis, Notes on error estimates for Galerkin approximations of the 'classical' Boussinesq system and related hyperbolic problems, Preprint, 2010. Available from: http://arxiv.org/abs/108.4248.
[8] D.C. Antonopoulos, V.A. Dougalis, D.E. Mitsotakis, Numerical solution of Boussinesq systems of the Bona-Smith family, Appl. Numer. Math. 60 (2010) 314–336.
[9] D.C. Antonopoulos, V.A. Dougalis, D.E. Mitsotakis, Initial-boundary-value problems for the Bona-Smith family of Boussinesq systems, Adv. Diff. Eqns. 14 (2009) 27–53.
[10] J.L. Bona, M. Chen, A Boussinesq system for two-way propagation of nonlinear dispersive waves, Physica D 116 (1998) 191–224.
[11] J.L. Bona, M. Chen, J.-C. Saut, Boussinesq equations and other systems for small-amplitude long waves in nonlinear dispersive media. I. Derivation and linear theory, J. Nonlin. Sci. 12 (2002) 283–318.
[12] J.L. Bona, M. Chen, J.-C. Saut, Boussinesq equations and other systems for small-amplitude long waves in nonlinear dispersive media. II. The nonlinear theory, Nonlinearity 17 (2004) 925–952.
[13] J.L. Bona, T. Colin, D. Lannes, Long wave approximations for water waves, Arch. Ration. Mech. Anal. 178 (2005) 373–410.
[14] J.L. Bona, V.A. Dougalis, O.A. Karakashian, W.R. McKinney, Conservative, high-order numerical schemes for the generalized Korteweg–de Vries equation, Philos. Trans. R. Soc. Lond. A 351 (1995) 107–164.
[15] J.L. Bona, V.A. Dougalis, D.E. Mitsotakis, Numerical solution of KdV–KdV systems of Boussinesq equations. I. The numerical scheme and generalized solitary waves, J. Math. Comput. Simul. 74 (2007) 214–228.
[16] J.L. Bona, V.A. Dougalis, D.E. Mitsotakis, Numerical solution of KdV–KdV systems of Boussinesq equations. II. Generation and evolution of radiating solitary waves, Nonlinearity 21 (2008) 2825–2848.
[17] J.G.B. Byatt-Smith, The reflection of a solitary wave by a vertical wall, J. Fluid Mech. 197 (1988) 503–521.
[18] M. Chen, Solitary-wave and multi-pulsed traveling-wave solutions of Boussinesq systems, Appl. Anal. 75 (2000) 213–240.
[19] W. Craig, P. Guyenne, J. Hammack, D. Henderson, C. Sulem, Solitary wave interactions, Phys. Fluids 18 (2006) 57–106.
[20] V.A. Dougalis, A. Duran, M.A. Lopez-Marcos, D.E. Mitsotakis, A numerical study of the stability of solitary waves of the Bona-Smith system, J. Nonlin. Sci. 17 (2007) 329–345.
[21] T. Dupont, Galerkin methods for first order hyperbolics: an example, SIAM J. Numer. Anal. 10 (1973) 890–899.
[22] A.S. Fokas, B. Pelloni, Boundary value problems for Boussinesq type systems, Math. Phys. Anal. Geom. 8 (2005) 59–96.
[23] D.E. Mitsotakis, Theory and numerical analysis of nonlinear dispersive wave equations: Boussinesq systems in one and two dimensions, Ph.D. Thesis, University of Athens, 2007 (in Greek).

[24] R.L. Pego, M.I. Weinstein, Convective linear stability of solitary waves for the Boussinesq equations, Stud. Appl. Math. 99 (1997) 311–375.
[25] B. Pelloni, Spectral methods for the numerical solution of nonlinear dispersive wave equations, Ph.D. Thesis, Yale University, 1996.
[26] B. Pelloni, V.A. Dougalis, Numerical modelling of two-way propagation of non-linear dispersive waves, J. Math. Comput. Simul. 55 (2001) 595–606.
[27] D.H. Peregrine, Calculations of the development of an undular bore, J. Fluid Mech. 25 (1966) 321–331.
[28] D.H. Peregrine, Long waves on a beach, J. Fluid Mech. 27 (1967) 815–827.
[29] D.H. Peregrine, Equations for water waves and the approximations behind them, in: R.E. Meyer (Ed.), Waves on Beaches and Resulting Sediment Transport, Academic Press, New York, 1972, pp. 95–121.
[30] M.E. Schonbek, Existence of solutions for the Boussinesq system of equations, J. Diff. Eqns. 42 (1981) 325–352.
[31] J. Scott Russel, Report on waves, in: 14th Meeting of the British Association for the Advancement of Science, John Murray, London, 1844, pp. 311–390.
[32] C.-H. Su, Q.-S. Zou, Waves generated by collisions of solitary waves, Phys. Rev. A 35 (1987) 4738–4742.
[33] G.B. Whitham, Linear and Nonlinear Waves, Wiley, New York, 1974.

Please cite this article in press as: D.C. Antonopoulos, V.A. Dougalis. Numerical solution of the ‘classical’ Boussinesq system, Math. Comput. Simul. (2011), doi:10.1016/j.matcom.2011.09.006